Given that downsizing is also advantageous, owing to its effect on reducing the toxicity and radiation burden to the host, we evaluated the radiolabeled Fab fragment. According to the in-vitro assays, radiolabeled Fabs bound specifically to H226 cells, similar to IgGs, and the affinity of radiolabeled Fabs was comparable to that of radiolabeled IgGs. Similar to parental IgG, radiolabeled Fabs also underwent internalization after binding with the antigen. Furthermore, we found a substantial amount of protein-bound fraction in the supernatant, which indicated detached Fab. This result may indicate the decreased binding affinity of the monovalent Fab compared with the divalent IgG, despite the high binding affinity of the Fab. Substantially decreased tumor uptake by ^{64}Cu-labeled or ^{111}In-labeled Fab in the H226 xenografts compared with that by ^{111}In-labeled IgG may reflect the decreased binding affinity of the Fab fragment. Although the tumor-to-blood ratio of radiolabeled Fab did not improve compared with radiolabeled IgG, sufficient tumor-to-blood ratios resulted at earlier times because the clearance of radiolabeled Fab from the blood was rapid. Using ^{64}Cu-labeled Fab, we could obtain a clear delineation of the tumor xenograft at 6 and 15 h after injection. Such results raise the possibility of ERC-specific imaging of patients with early-stage mesothelioma by PET using ^{64}Cu-DOTA-Fab. The uptake of radiolabeled Fabs with metal radionuclides in the kidney was extremely high, which is similar to other Fabs. To counteract this adverse result, the development of a new labeling method with metal radionuclide to decrease renal uptake, such as ^{131}I-iodohippuryl N(ε)-maleoyl-L-lysine, is required [18].

Although we successfully visualized the ERC-expressing xenografted tumor, H226, by ^{64}Cu-DOTA-Fab, tumor uptake seems to be insufficient for clinical application despite high affinity *in vitro*. The H226 cells highly expressed ERC *in vitro*, but the ERC expression of the H226 xenografts was apparently lower than human mesothelioma according to earlier studies [6,12]. Epithelioid mesothelioma in patients forms tubulopapillary architectures and strongly expresses ERC on its surface. However, the H226 tumors used in this study were poorly differentiated compared with typical epithelioid mesothelioma in humans. The discrepancy between in-vitro and in-vivo results in H226 might come from high expression of ERC *in vitro* and low expression *in vivo*. Conversely, the uptake of radiolabeled antibodies in H226 tumors was significantly higher than that in 211H tumors, in which C-ERC expression was not determined by immunohistochemistry [12]. These findings raise the possibility that ^{64}Cu-DOTA-Fab could detect small-sized mesothelioma at an early stage. The use of a model showing higher in-vivo ERC expression may further confirm the potential of this antibody, in addition to improvement in binding affinity. Future research should therefore aim to improve the affinity/avidity of this antibody, for example through the use of divalent scFv [21], and to establish a more clinically relevant tumor model, which forms tubulopapillary architectures and strongly expresses ERC in tumors, to evaluate this antibody before conducting a clinical study.

Conclusion

We evaluated the affinity of radiolabeled IgG and Fab for C-ERC *in vitro* and *in vivo* for use as an imaging probe for mesothelioma-expressing ERC, which is expressed in early-stage mesothelioma. ERC-expressing xenografted tumors could be visualized in nude mice by PET imaging with ^{64}Cu-DOTA-Fab. Our findings suggest that ERC-specific imaging using a positron-emitting radiopharmaceutical ^{64}Cu-DOTA-Fab could be used to diagnose patients with early-stage mesothelioma.

Acknowledgements

We thank Kenichi Odaka for technical advice and help with single-photon emission computed tomography; Hisashi Suzuki, Masami Fukada, and Francisco Lazaro Guerra Gomez for ^{64}Cu production; staff in the Cyclotron Operation section for the cyclotron operation; Yuriko Ogawa for technical assistance; Hidekatsu Wakizaka for the operation and quality control of the PET scanner; and Yoshi-nobu Harada for encouragement.

References

1 Robinson BW, Lake RA. Advances in malignant mesothelioma. *N Engl J Med* 2005; **353**:1591–1603.
2 Tsiouris A, Walesby RK. Malignant pleural mesothelioma: current concepts in treatment. *Nat Clin Pract Oncol* 2007; **4**:344–352.
3 Kanazawa N, Ioka A, Tsukuma H, Ajiki W, Oshima A. Incidence and survival of mesothelioma in Osaka, Japan. *Jpn J Clin Oncol* 2006; **36**:254–257.
4 Peto J, Decarli A, La Vecchia C, Levi F, Negri E. The European mesothelioma epidemic. *Br J Cancer* 1999; **79**:666–672.
5 Sugarbaker DJ, Flores RM, Jaklitsch MT, Richards WG, Strauss GM, Corson JM, *et al.* Resection margins, extrapleural nodal status, and cell type determine postoperative long-term survival in trimodality therapy of malignant pleural mesothelioma: results in 183 patients. *J Thorac Cardiovasc Surg* 1999; **117**:54–63. Discussion-5.
6 Maeda M, Hino O. Molecular tumor markers for asbestos-related mesothelioma: serum diagnostic markers. *Pathol Int* 2006; **56**:649–654.
7 Ishikawa K, Segawa T, Hagiwara Y, Maeda M, Abe M, Hino O. Establishment of novel mAb to human ERC/mesothelin useful for study and diagnosis of ERC/mesothelin-expressing cancers. *Pathol Int* 2009; **59**:161–166.
8 Shiomi K, Hagiwara Y, Sonoue K, Segawa T, Miyashita K, Maeda M, *et al.* Sensitive and specific new enzyme-linked immunosorbent assay for N-ERC/mesothelin increases its potential as a useful serum tumor marker for mesothelioma. *Clin Cancer Res* 2008; **14**:1431–1437.
9 Hassan R, Wu C, Brechbiel MW, Margulies I, Kreitman RJ, Pastan I. 111Indium-labeled monoclonal antibody K1: biodistribution study in nude mice bearing a human carcinoma xenograft expressing mesothelin. *Int J Cancer* 1999; **80**:559–563.
10 Sato N, Hassan R, Axworthy DB, Wong KJ, Yu S, Theodore LJ, *et al.* Pretargeted radioimmunotherapy of mesothelin-expressing cancer using a tetravalent single-chain Fv-streptavidin fusion protein. *J Nucl Med* 2005; **46**:1201–1209.
11 Kreitman RJ, Hassan R, Fitzgerald DJ, Pastan I. Phase I trial of continuous infusion anti-mesothelin recombinant immunotoxin SS1P. *Clin Cancer Res* 2009; **15**:5274–5279.
12 Tsuji AB, Sogawa C, Sugyo A, Sudo H, Toyohara J, Koizumi M, *et al.* Comparison of conventional and novel PET tracers for imaging

mesothelioma in nude mice with subcutaneous and intrapleural xenografts. *Nucl Med Biol* 2009; **36**:379–388.
13 McCarthy DW, Shefer RE, Klinkowstein RE, Bass LA, Margeneau WH, Cutler CS, *et al.* Efficient production of high specific activity 64Cu using a biomedical cyclotron. *Nucl Med Biol* 1997; **24**:35–43.
14 Saga T, Sakahara H, Yao Z, Nakamoto Y, Sato N, Hattori N, *et al.* Detection of altered adhesion molecule expression in experimental tumors by a radiolabeled monoclonal antibody. *Jpn J Cancer Res* 1997; **88**:1171–1180.
15 Lindmo T, Boven E, Cuttitta F, Fedorko J, Bunn PA Jr. Determination of the immunoreactive fraction of radiolabeled monoclonal antibodies by linear extrapolation to binding at infinite antigen excess. *J Immunol Methods* 1984; **72**:77–89.
16 Saga T, Endo K, Akiyama T, Sakahara H, Koizumi M, Watanabe Y, *et al.* Scintigraphic detection of overexpressed c-erbB-2 protooncogene products by a class-switched murine anti-c-erbB-2 protein monoclonal antibody. *Cancer Res* 1991; **51**:990–994.
17 Sharkey RM, Goldenberg DM. Perspectives on cancer therapy with radiolabeled monoclonal antibodies. *J Nucl Med* 2005; **46 (Suppl 1)**: 115S–127S.
18 Arano Y, Fujioka Y, Akizawa H, Ono M, Uehara T, Wakisaka K, *et al.* Chemical design of radiolabeled antibody fragments for low renal radioactivity levels. *Cancer Res* 1999; **59**:128–134.
19 Becker WS, Behr TM, Cumme F, Rossler W, Wendler J, Kern PM, *et al.* ^{67}Ga citrate versus ^{99m}Tc-labeled LL2-Fab' (anti-CD22) fragments in the staging of B-cell non-Hodgkin's lymphoma. *Cancer Res* 1995; **55**:5771s–5773s.
20 Uehara T, Koike M, Nakata H, Hanaoka H, Iida Y, Hashimoto K, *et al.* Design, synthesis, and evaluation of [^{188}Re]organorhenium-labeled antibody fragments with renal enzyme-cleavable linkage for low renal radioactivity levels. *Bioconjug Chem* 2007; **18**:190–198.
21 Holliger P, Hudson PJ. Engineered antibody fragments and the rise of single domains. *Nat Biotechnol* 2005; **23**:1126–1136.

YGENO-08182; No. of pages: 7; 4C: 3, 6

Genomics xxx (2010) xxx–xxx

Contents lists available at ScienceDirect

Genomics

journal homepage: www.elsevier.com/locate/ygeno

Knockdown of *COPA*, Identified by Loss-of-Function Screen, Induces Apoptosis and Suppresses Tumor Growth in Mesothelioma Mouse Model

Hitomi Sudo [a,b], Atsushi B. Tsuji [a,*], Aya Sugyo [a], Masakazu Kohda [c], Chizuru Sogawa [a], Chisato Yoshida [a], Yoshi-nobu Harada [a], Okio Hino [b], Tsuneo Saga [a]

[a] Diagnostic Imaging Group, Molecular Imaging Center, National Institute of Radiological Sciences, 4-9-1 Anagawa, Inage-ku, Chiba 263-8555, Japan
[b] Department of Pathology and Oncology, Juntendo University School of Medicine, 2-1-1 Hongo, Bunkyo-ku, Tokyo, 113-8421, Japan
[c] Division of Functional Genomics and Systems Medicine, Research Center for Genomic Medicine, Saitama Medical University, 1397-1 Yamane, Hidaka-shi, Saitama 350-1241, Japan

ARTICLE INFO

Article history:
Received 28 August 2009
Accepted 3 February 2010
Available online xxxx

Keywords:
RNAi
Functional screening
Cell proliferation
Mesothelioma
Apoptosis

ABSTRACT

Malignant mesothelioma is a highly aggressive tumor arising from serosal surfaces of the pleura and is triggered by past exposure to asbestos. Currently, there is no widely accepted treatment for mesothelioma. Development of effective drug treatments for human cancers requires identification of therapeutic molecular targets. We therefore conducted a large-scale functional screening of mesothelioma cells using a genome-wide small interfering RNA library. We determined that knockdown of 39 genes suppressed mesothelioma cell proliferation. At least seven of the 39 genes—*COPA, COPB2, EIF3D, POLR2A, PSMA6, RBM8A,* and *RPL18A*—would be involved in anti-apoptotic function. In particular, the COPA protein was highly expressed in some mesothelioma cell lines but not in a pleural mesothelial cell line. *COPA* knockdown induced apoptosis and suppressed tumor growth in a mesothelioma mouse model. Therefore, *COPA* may have the potential of a therapeutic target and a new diagnostic marker of mesothelioma.

Introduction

Malignant mesothelioma is a highly aggressive tumor arising from the serosal surfaces of the pleura, peritoneum, and pericardium [1,2]. About 75% of all cases involve the pleura, and the remaining involve the peritoneum or pericardium. Mesothelioma is associated with previous asbestos exposure with a latency of 30–40 years. The three main categories of mesothelioma are epithelioid (50–70% of all cases), sarcomatoid (7–20%), and mixed/biphasic (20–30%). This tumor was once rare, but the incidence is expected to increase worldwide over the next several decades as a result of widespread asbestos exposure, both occupational and environmental, in many countries [2–4].

Current treatments include some form of surgery, which may be combined with chemotherapy and/or radiation. However, the prognosis of patients with this multimodality therapy remains poor, with typical post-diagnosis survival being 8–18 months [1,2]. Significantly, traditional chemotherapy has yielded poor response rates (typically <15–20%) [1,2]. Thus, the lack of a highly effective therapeutic regimen for mesothelioma underscores the importance of finding new and more effective treatments.

To develop effective drugs for treatment of human cancer, it is important to identify therapeutic target molecules. Small interfering RNAs (siRNA) have been widely used in mammalian cells to define the functional roles of individual genes, particularly in disease. In addition, the development of whole-genome siRNA libraries and use of high throughput loss-of-function screens have allowed systematic detection of genes required for disease processes such as cancer [5–7]. We previously established a high-throughput screening procedure [8,9] and performed a large-scale screening to identify radiation-susceptible genes [9]. In the present study, we screened potential drug target molecules in mesothelioma cells using the high-throughput screening assay with a genome-wide siRNA library, containing small double-stranded RNAs targeted to more than 8,500 human genes, and conducted *in vitro* and *in vivo* functional analysis of several genes identified by this screening.

Results

Primary screening

The siRNA library used in this study contained 8,589 siRNAs consisting of nine sub-libraries: ion binding, ion channel, kinase, membrane transporter, nucleic acid binding, phosphatase, receptor, transcription factor, and transporter (Table 1) in a 96-well format. We performed primary screening by transfecting each siRNA individually into human malignant mesothelioma cells 211H [10] and measured the remaining viable cells at four days after transfection as determined by a sulforhodamine B-based cell proliferation assay [8,9]. Following gene-specific siRNA transfection, we identified 383 genes for which <50% viable cells remained compared with mock-

* Corresponding author. Fax: +81 43 206 4138.
E-mail address: a_tsuji@nirs.go.jp (A.B. Tsuji).

0888-7543/$ – see front matter © 2010 Elsevier Inc. All rights reserved.
doi:10.1016/j.ygeno.2010.02.002

Table 1
Summary of genes in the siRNA library and results of the first screen using MSTO-211H mesothelioma cell line.

Library name	Number of genes in library	Genes showing reduced viability	
		<20%[a]	2-500%[a]
Ion binding	1,479	5	23
Ion channel	349	0	2
Kinase	800	5	24
Membrane Transporter	695	0	12
Nucleic acid binding	1,951	39	117
Phosphatase	599	0	3
Receptor	1,425	16	69
Transcription factor	995	7	36
Transporter	296	6	19
Total	8,589	78	305

[a] % viable cells compared with mock transfected cells.

transfected cells (Table 1 and Supplementary Table 1). Of the 383 genes, 78 showed viability of <20%. These 78 most-effective genes had the following functional distribution: ion binding (5), kinase (5), nucleic acid binding (39), receptor (16), transcription factor (7), and transporter (6) (Table 1 and Supplementary Table 1).

Secondary screening

We synthesized additional siRNAs against the 78 genes identified in the primary screening and built an original sub-library containing 156 siRNAs (two distinct siRNAs for each gene) against these 78 genes in the 96-well format. Knockdown of each gene was achieved by each of two distinct gene-specific siRNAs, and we measured viable cells at 2, 4, and 6 days after transfection. For 39 genes, *COPA, COPB2, EIF3D, POLR2A, PSMA6, RBM8A, RPL18A, OR52I1, RPA1, EIF3C, WEE1, RPL8, RPL3, RPL19, EIF3A, RPS2, RPL6, SF3B1, KISS1R, EIF3I, LSM2, RPL4, RPL21, POLR2F, RPL27A, RPL7, SF3B4, RPL5, RPS18, RPLP1, RPL18, KPNB1, EIF3E, SF3B14, RPL11, EIF3G, RPL35A, RPS17,* and *SNRNP200*, both siRNAs reduced cell viability compared with the negative control (Figs. 1A and B, and Supplementary Fig. 1). For 20 other genes, *TBRG1, DIS3, OR2T27, RPS19, SETD1A, RFX3, PHF5A, EPS8L3, MAX, ASCL2, LCE3A, ZC3H8, C9orf98, WWOX, ITPKA, FCGR3B, NDUFAF2, SCAND3, CAT,* and *RXRG*, only one siRNA reduced cell viability (Supplementary Fig. 1).

Apoptosis assay of mesothelioma cells transfected with siRNAs against seven genes

Based on the greatest negative impact on cell viability of siRNA-mediated knockdown of genes in our screen and their functional categories, we selected seven representative genes, *COPA, COPB2, EIF3D, POLR2A, PSMA6, RBM8A,* and *RPL18A*, for further analysis of their contribution to apoptosis. On treatment with specific siRNAs, the expression of these seven genes was reduced to < 10% compared with the negative control, as assessed by real-time RT-PCR (Fig. 1C). We first stained nuclei of knockdown cells with Hoechst 33342 at 48 h after transfection and observed them under the fluorescence microscope. Apoptosis in cell populations transfected with gene-specific siRNAs targeting the seven selected genes apparently increased compared with cells transfected with the negative control siRNA (data not shown). Using flow cytometry, we then measured annexin V-positive apoptotic cells at 8, 24, and 48 h after transfection (Fig. 2). In the negative control, the apoptotic population was not increased at any time point after transfection. At 24 h after transfection, cells transfected with siRNAs targeting five genes, *EIF3D, POLR2A, PSMA6, RBM8A,* and *RPL18A*, contained significantly more apoptotic cells compared with the negative control ($P<0.01$, Fig. 2B), whereas cells transfected with *COPA* and *COPB2* siRNAs did not. At 48 h after transfection, the apoptotic population in all seven of the gene-knockdown cells was significantly increased compared with the negative control ($P<0.01$; Figs. 2A and B). Among cells transfected with the negative control or gene-specific siRNAs, the necrotic population of cells (negative for annexin V and positive for 7-AAD) was not increased at any time point (data not shown).

Functional analysis of COPA in mesothelioma cells

Among these 7 genes, because the *COPA* mRNA has been previously reported to be highly expressed in mesothelioma compared with normal tissues (tumor/normal ratio was 2.19) by microarray experiments [12], we focused on further functional analysis of COPA. To determine whether COPA protein is expressed in mesothelioma, we conducted immunoblotting analysis in four mesothelioma cell lines, 211H, H226, H2052, and H2452, and the pleural mesothelial cell line, MeT-5A. COPA protein was highly expressed in 211H, H2052, and H2452 cells, but not in H226 and MeT-5A cells (Fig. 3A). We examined the ability of *COPA* siRNAs to downregulate *COPA* mRNA in mesothelioma and the pleural mesothelial cell lines by real-time RT-PCR. At 24 h after siRNA-transfection, both siRNAs reduced *COPA* mRNA to <10% in 211H cells compared with the negative control siRNA (Fig. 1C). In H2052 and Met-5A cells, *COPA* mRNAs were reduced to <40% compared with control (Fig. 3B). In H226 and H2452 cells, *COPA* siRNAs were insufficient to reduce *COPA* mRNAs compared with negative control (>60%; Fig. 3B). We then performed cell proliferation assay of *COPA* siRNA-transfected 211H, H2052, and MeT-5A. Both siRNAs (COPAsi1 and COPAsi2) reduced cell viability significantly to <10% (5.4 and 4.6%) and <35% (19.2 and 31.7%) in 211H and H2052, respectively, compared with the negative control, whereas *COPA* siRNA-transfected MeT-5A cells survived >60% (67.1 and 61.2%) compared with control (Fig. 3C).

COPA siRNA treatment in a mesothelioma mouse model

To examine whether *COPA* siRNAs suppress tumor growth in a mesothelioma mouse model, we first conducted treatment experiments with the pretreatment protocol in which 211H cells transfected with *COPA* or negative control siRNAs were subcutaneously injected into nude mice. Fig. 4A shows that negative control siRNA-transfected cells formed tumors that grew linearly with time, whereas 211H cells transfected with both *COPA* siRNAs formed tumors with significant reductions in tumor growth compared with the negative control ($P<0.01$). Second, we conducted a local injection protocol in nude mice bearing 211H xenografts. The untreated 211H cells were subcutaneously inoculated into nude mice, and *COPA* or negative control siRNAs were injected around xenografts twice. The treatment of both *COPA* siRNAs caused significant inhibition in tumor growth compared with the negative control siRNA ($P<0.05$; Fig. 4B).

Fig. 1. Cell viability and gene expression analysis of 211H transfected with seven genes, *COPA, COPB2, EIF3D, POLR2A, PSMA6, RBM8A,* and *RPL18A*. (A) Cell viability of 211H cells transfected with 14 siRNAs against seven genes selected by primary screening shown in Supplementary Table 1 and the negative control siRNA. Cell viability about more 71 genes were shown in Supplementary Fig. 1. Cell viability was measured by sulforhodamine B-based cell proliferation assay at 2, 4, and 6 days after transfection. Data represent mean ± SD from three independent experiments. Open circles represent cells transfected with negative control siRNA, closed squares represent gene-specific siRNA (si1) for each gene, and closed triangles represent gene-specific siRNA (si2) for each gene. (B) Representative sulforhodamine B-stained cells at 2, 4, and 6 days after transfection. Cells transfected with negative control siRNA or gene-specific siRNAs targeting seven genes. (C) Gene expression analysis of 211H cells transfected with siRNAs. The cDNAs were directly synthesized from cells at 24 h after transfection with either negative control siRNA or gene-specific siRNAs targeting seven genes. Gene expression was determined by real-time RT-PCR with TaqMan probes. The expression level of each target gene was normalized to that of 18S ribosomal RNA. Data represent mean and SD from three independent experiments.

Please cite this article as: H. Sudo, et al., Knockdown of *COPA*, Identified by Loss-of-Function Screen, Induces Apoptosis and Suppresses Tumor Growth in Mesothelioma Mouse Model, Genomics (2010), doi:10.1016/j.ygeno.2010.02.002

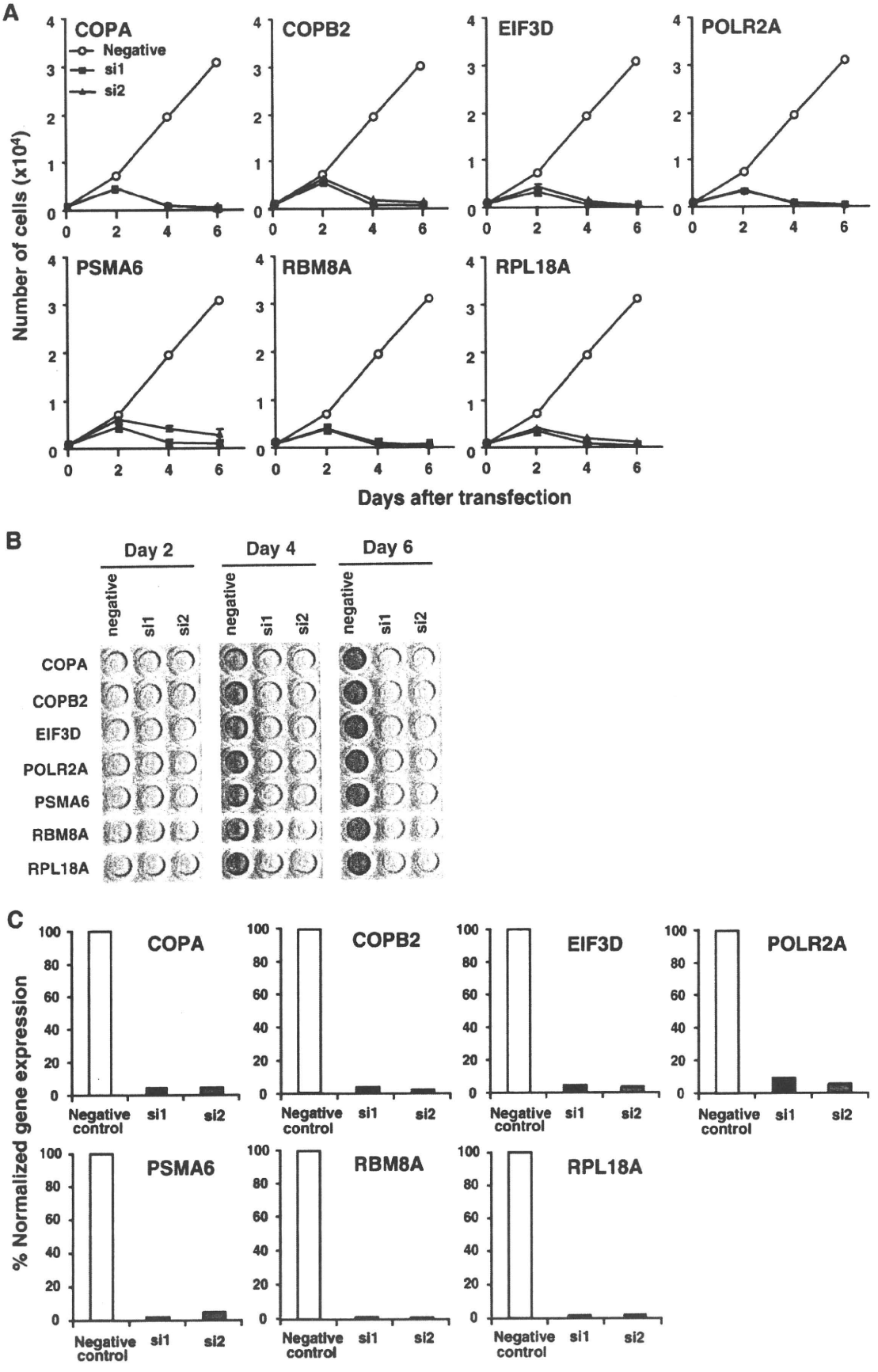

Please cite this article as: H. Sudo, et al., Knockdown of *COPA*, Identified by Loss-of-Function Screen, Induces Apoptosis and Suppresses Tumor Growth in Mesothelioma Mouse Model, Genomics (2010), doi:10.1016/j.ygeno.2010.02.002

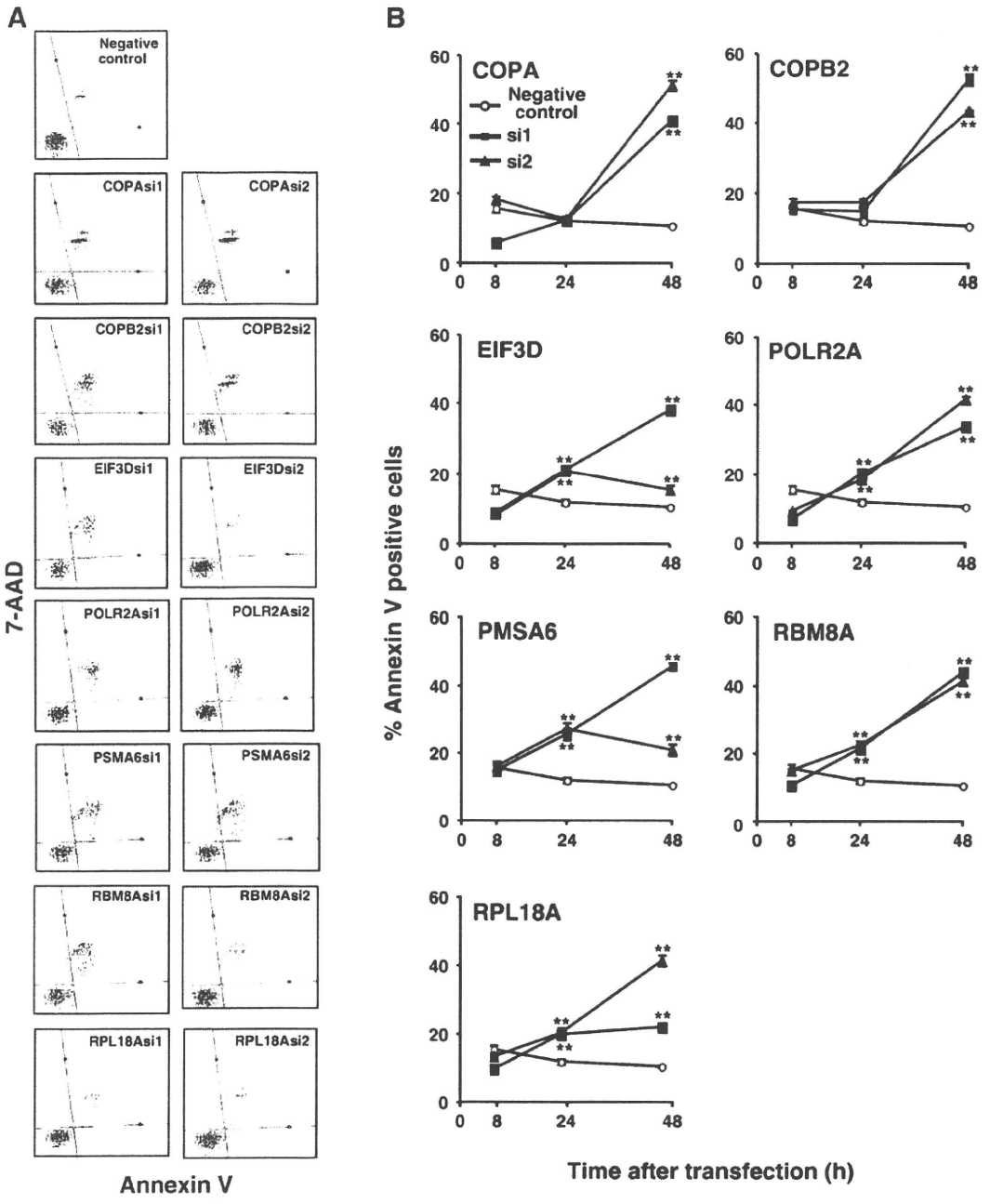

Fig. 2. Apoptotic analysis of 211H cells transfected with seven individual siRNAs against *COPA, COPB2, ELF3D, POLR2A, PSMA6, RBM8A,* and *RPL18A* and stained with annexin V and 7-amino-actinomycin D (7-AAD, DNA staining) at 8, 24, and 48 h after transfection. Living (annexin V negative and 7-AAD negative), necrotic (annexin V negative and 7-AAD positive), and apoptotic (annexin V positive) cells were determined by a Guava PCA system. (A) Representative flow cytometry dot plots at 48 h after transfection. (B) Mean percentage values of apoptotic cell from three independent experiments, as analyzed by ANOVA with the Student–Newman–Keuls method multiple comparison test (vs. negative control, $^{**}P<0.01$). Data are presented as means ± SD from three independent experiments. Open circles represent cells transfected with negative control siRNA, closed squares represent gene-specific siRNA (si1) of each gene, and closed triangles represent gene-specific siRNA (si2) of each gene.

Immunohistochemical staining of 211H xenografted tumors was performed two days after second injection of siRNAs to evaluate apoptosis. We observed a marked increase of apoptotic cells in tumors treated with both *COPA* siRNAs compared with the negative control (Fig. 4C). From quantitative analysis of immunohistochemical staining, both *COPA* siRNAs caused 12- and 10-fold increases of TUNEL-positive cells, respectively, compared with the negative control siRNA ($P<0.01$; Fig. 4D).

Discussion

We report here for the first time a large-scale loss-of-function screening to identify potential drug target molecules for mesothelioma treatments. We conducted a large-scale functional screening of a mesothelioma cell line, 211H, using a genome-wide siRNA library to identify potential drug target molecules. Of siRNAs to 383 genes that reduced mesothelioma cell viability by at least 50%, siRNAs to 78

Please cite this article as: H. Sudo, et al., Knockdown of *COPA*, Identified by Loss-of-Function Screen, Induces Apoptosis and Suppresses Tumor Growth in Mesothelioma Mouse Model, Genomics (2010), doi:10.1016/j.ygeno.2010.02.002

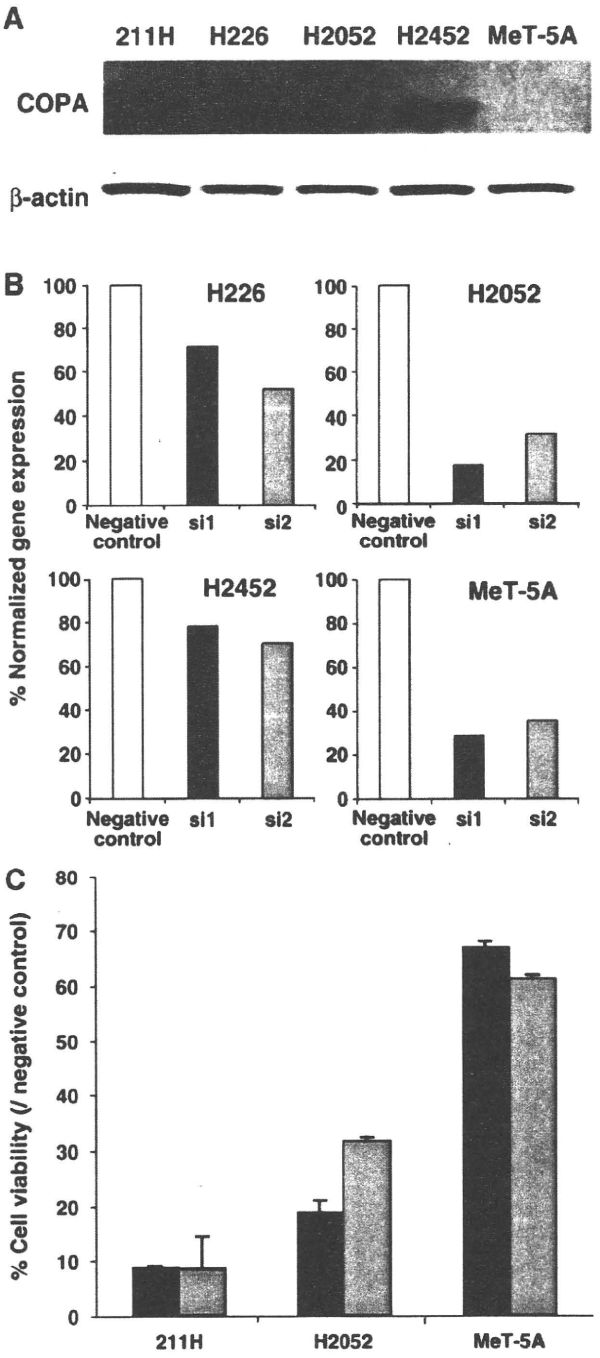

Fig. 3. *COPA* expression in mesothelioma cell lines and cell proliferation of *COPA* siRNA-transfected cells. (A) COPA protein expressions were detected by immunoblot analysis in mesothelioma cell lines (211H, H226, H2052, and H2452) and pleural mesothelial cell line (MET-5A). (B) Expression of *COPA* mRNA was determined by real-time RT-PCR with TaqMan probes. Data represent mean and SD from three independent experiments. (C) Cell proliferation assay of *COPA* siRNA-transfected cells. Data are presented as means and SD from three independent experiments.

genes decreased viability by at least 80%, raising the possibility that these genes regulate cell viability in mesothelioma. To further explore this possibility, we newly synthesized and built an original sub-library containing 156 siRNAs against the above-mentioned 78 genes and assessed the effect of gene silencing on cell viability. Of these 78 genes, we found 39 genes that reduced cell viability at 4 and/or 6 days after transfection with gene-specific siRNAs, suggesting a crucial role for these genes in mesothelioma cell viability and as potential drug targets for treatment. We focused on further functional studies of these 39 genes (mentioned below). For additional 22 genes, cell viability was reduced by one but not both gene-specific siRNAs. This result cannot conclusively establish whether the lack of significant reduction of viable cells resulted from insufficient knockdown in either siRNA or whether the result reflected an off-target effect [7,11]. To clearly identify which of these genes could be associated with cell viability in mesothelioma will require further investigation using additional siRNAs.

Of the 39 genes detected by this screening, almost all cells transfected with siRNAs died at 4 and/or 6 days after transfection. To determine whether apoptosis caused this cell death, we chose seven representative genes, *COPA, COPB2, EIF3D, POLR2A, PSMA6, RBM8A,* and *RPL18A*, based on the greatest negative impact on cell viability of siRNA-mediated knockdown of genes in our screen and their functional categories. According the apoptosis assay of knockdown cells using microscopic and flow cytometric analyses, apoptosis of cell populations targeted with gene-specific siRNAs for each of the seven genes was significantly increased compared with cells with the negative control siRNA. This suggests that these genes can be involved in anti-apoptotic function. Interestingly, *COPA, COPB2, EIF3D,* and *PBM8A* have not been known to be associated with apoptosis. Thus, further investigation of these genes may lead to the elucidation of new molecular mechanisms of apoptosis.

The *COPA* mRNA has been previously reported to be highly expressed in mesothelioma compared with normal tissues [12]. To examine COPA protein expression in mesothelioma cells, we performed immunoblotting analysis for four mesothelioma cell lines (211H, H226, H2052, and H2452) and the pleural mesothelial cell line (MeT-5A). The COPA protein is highly expressed in 211H, H2052, and H2452 cells, but not in H226 and MeT-5A cells. This result suggests that *COPA* could be a new therapeutic target for mesotheliomas that highly express *COPA*. To test this possibility, we conducted cell proliferation assay in 211H, H2052, and MeT-5A cells, in which *COPA* siRNAs were sufficient to reduce *COPA* mRNAs for the assay. *COPA* siRNAs markedly reduced cell viability to <10% and <35% in 211H and H2052 cells, respectively, compared with the negative control, whereas MeT-5A cells survived >60%. We treated mesothelioma mouse models using *COPA* siRNAs with both protocols (pretreatment and local injection) and clearly showed that *COPA* siRNAs suppressed tumor growth and induced apoptosis. The pretreatment protocol was more effective than the local injection protocol. Because the transfection efficiency of mesothelioma cells in dishes is expected to be higher than that in mice, this result was probably due to the transfection efficiency of *COPA* siRNAs. If we could find a small inhibitor molecule of *COPA*, it would help clarify this point and be a potential drug compound for treatment of mesotheliomas that highly express *COPA*.

COPA is one of the seven non-clathrin-coated vesicular coat subunits that form the "coatomer," which plays a role in membrane transport between the endoplasmic reticulum and the Golgi apparatus [13,14]. *COPA* and *COPB2* have a tryptophan-aspartic acid (WD)-repeat motif and belong to a large conserved family of WD proteins found in all eukaryotes and implicated in a variety of functions ranging from signal transduction and transcriptional regulation to cell cycle control and apoptosis [15]. This report and our present results suggest that *COPA* and *COPB2* could play a role not only in membrane transport but also in apoptosis. Thus, further study of *COPA* and *COPB2* might help elucidate the molecular mechanism of apoptosis. *COPA* and *COPB2* have been reported to interact with platelet-derived growth factor β-receptor [16], which is a cell surface tyrosine kinase receptor, binds SH2 domain containing proteins, activates cell growth signaling, and is related to angiogenesis [17,18]. Tumor angiogenesis is a critical step in tumor development through which tumors establish independent nutrient and oxygen supply, consequently enhancing tumor

Please cite this article as: H. Sudo, et al., Knockdown of *COPA*, Identified by Loss-of-Function Screen, Induces Apoptosis and Suppresses Tumor Growth in Mesothelioma Mouse Model, Genomics (2010), doi:10.1016/j.ygeno.2010.02.002

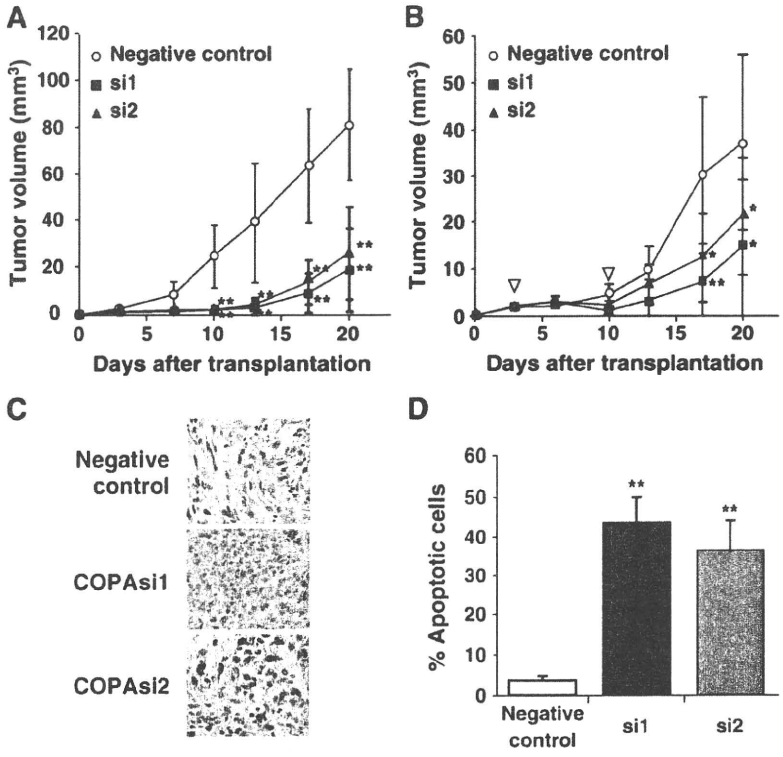

Fig. 4. Therapeutic efficacy of *COPA* siRNA *in vivo*. (A) For the pretreatment protocol, siRNA-transfected 211H cells were injected subcutaneously into nude mice, and tumor diameters were measured at a regular interval for up to 20 days and tumor volume was calculated. Results represent mean ± SD (n = 5) compared with negative control (**$P<0.01$). Open circles represent cells transfected with negative control siRNA, closed squares represent gene-specific siRNA (si1), and closed triangles represent gene-specific siRNA (si2). (B) For the local injection protocol, 3 and 10 days after inoculation of 211H cells, 10 nmol of *COPA* siRNAs or negative control siRNA was mixed with atelocollagen, and 100 μl of each mixture was injected around tumor. Tumor diameters were measured at a regular interval for up to 20 days and tumor volume was calculated. Results represent the mean ± SD (n = 4 tumors) compared with negative control (*$P<0.05$, **$P<0.01$). Open triangles represent siRNA injection. (C) The effect of *COPA* siRNA on apoptosis *in vivo*. Immunohistochemical analysis of 211H tumor xenografts stained with TUNEL (Magnification, 400×, Size bar, 50 μm). (D) The ratio of the apoptotic cells. Data are presented as mean ± SD compared with negative control (**$P<0.01$).

growth. *COPA* was highly expressed in some mesotheliomas according to our results and the previous report [12]. These findings suggest that *COPA* over-expression could play a role in mesothelioma development through anti-apoptosis and/or angiogenesis. Further studies would be important to explore the correlation between mesothelioma development and potential roles of *COPA* in anti-apoptosis and/or angiogenesis.

In conclusion, we conducted a large-scale functional screening in mesothelioma cells using a genome-wide siRNA library and determined that knockdown of 39 genes suppressed cell proliferation of mesothelioma cells, at least seven of which—*COPA, COPB2, EIF3D, POLR2A, PSMA6, RBM8A*, and *RPL18A*—are associated with an anti-apoptotic function. Functional characterization of these genes and their role in apoptosis pathways may provide clues to the underlying molecular mechanisms of cell death as well as to the development of novel therapeutic agents for mesothelioma. In particular, *COPA* may hold promise for the development of new therapy for malignant mesothelioma that highly express *COPA*.

Materials and methods

Cell culture

We obtained human malignant mesothelioma cell lines, 211H [10], H226, H2052, and H2452, and the human pleural mesothelial cell line MeT-5A from American Type Culture Collections (Manassas, VA). Cells were maintained in RPMI 1640 medium (Sigma, St. Louis, MO) supplemented with 5% fetal calf serum (JRH Biosciences, Lenexa, KS).

SiRNA library

We purchased a human genome-wide siRNA library (siPerfect Library; RNAi Co., Ltd, Tokyo, Japan) containing small double-stranded RNAs against 8,589 human genes. This library consists of nine sub-libraries: ion binding, ion channel, kinase, membrane transporter, nucleic acid binding, phosphatase, receptor, transcription factor, and transporter. We also purchased a negative control siRNA and additional gene-specific siRNAs custom-synthesized by RNAi Co., Ltd.

Cell proliferation assay

We seeded 1.5×10^3 cells in each well of 96-well plates and transfected them with siRNA (5 nM) using Lipofectamine 2000 reagent (Invitrogen, Carlsbad, CA). After 4 days, we performed cell proliferation assay using a sulforhodamine B-based Toxicology Assay kit (Sigma) as reported previously [8,9]. We estimated the numbers of cells based on a standard curve obtained by serial dilutions (10^4 to 625 cells).

Real-time quantitative reverse transcriptase-PCR

We seeded 1.5×10^5 cells in a 3-cm dish and transfected them with siRNA (5 nM). After 24 h, we synthesized first-strand cDNAs from knockdown cells using the FastLane Cell cDNA kit (Qiagen, Hilden, Germany). Predesigned and preoptimized TaqMan probes to detect genes of interest and 18S ribosomal RNA were purchased from Applied Biosystems (Foster City, CA). Real-time reverse transcriptase-PCR (RT-PCR) was performed in triplicate using a Premix Ex Taq

Please cite this article as: H. Sudo, et al., Knockdown of *COPA*, Identified by Loss-of-Function Screen, Induces Apoptosis and Suppresses Tumor Growth in Mesothelioma Mouse Model, Genomics (2010), doi:10.1016/j.ygeno.2010.02.002

reagent (Takara-Bio, Otsu, Japan) on a Mx3000 (Stratagene, La Jolla, CA) real-time PCR instrument. Gene expression levels were normalized to 18S ribosomal RNA expression in each sample.

Apoptosis analysis with Hoechst 33342 staining

We seeded 1.5×10^5 cells in a 6-cm dish and transfected them with siRNAs (10 nM). After 48 h, we added Hoechst 33342 (3 μl; 1 μg/ml; Dojindo Laboratories, Kumamoto, Japan) to the culture medium and incubated the cells for 60 min. The culture medium was then removed and replaced with fresh medium. We observed the stained cells under a fluorescence microscope (Olympus, Tokyo, Japan).

Apoptosis analysis with annexin V staining

We transfected 1.5×10^5 cells with siRNAs (10 nM) and harvested them for 8, 24, and 48 h. The cells were stained with annexin V and 7-amino-actinomycin D (7-AAD) using a Guava PCA Nexin kit (Guava Technologies, Hayward, CA) as described previously [9]. We counted 2,500 events and identified living (annexin V negative, 7-AAD negative), apoptotic (annexin V positive, 7-AAD positive and negative), and necrotic cells (annexin V negative, 7-AAD positive) by a Guava PCA system (Guava Technologies). Data were analyzed by ANOVA with the Student–Newman–Keuls method multiple comparison test.

Immunoblot analysis

We lysed cells in a buffer containing 20 mM Tris-HCl (pH 7.5), 150 mM NaCl, 1 mM EDTA, 1 mM EGTA, 1% Triton X-100, 2.5 mM sodium pyrophosphate, 1 mM β-glycerophosphate, 1 mM Na_3VO_4, 1 μg/ml leupeptin, and 0.2 M 4-(2-Aminoethyl)-benzenesulfonyl fluoride hydrochloride. We estimated the protein concentration using the Quick Start Bradford Protein Assay kit (Bio-Rad, Hercules, CA). Cell lysates (40 μg) were separated by sodium dodecyl sulfate-polyacrylamide gel electrophoresis, transferred to polyvinylidene difluoride membranes using the iBlot Dry Blotting System (Invitrogen), and probed with anti-COPA polyclonal (Abcam, Cambridge, UK) or anti-β-actin monoclonal (Sigma) antibodies. We detected the primary antibodies using horseradish peroxidase-linked goat anti-mouse or anti-rabbit IgG (GE Healthcare, Little Chalfont, UK) and visualized them by the ECL Plus kit (GE Healthcare).

COPA siRNA treatment in mesothelioma mouse models

We obtained female nude mice (BALB/c-nu/nu, 5–6 weeks old) from CLEA Japan (Tokyo, Japan) and maintained them under specific pathogen-free conditions. For a pretreatment protocol, we transfected 211H cells (2×10^6) with COPA-specific (si1 or si2) or control siRNAs, and 24 h later we implanted the cells subcutaneously into the nude mice under ether anesthesia. The size of subcutaneous tumor was measured twice a week using a caliper. Tumor volume was calculated using the following formula: tumor volume (mm^3) = $(W \times H \times D)/2$, where W is width, H is height, and D is depth in millimeters. For a local injection protocol, we implanted 2×10^6 of 211H cells subcutaneously into nude mice under ether anesthesia. We treated the tumor-bearing nude mice with 10 nmol of COPA-specific (si1 or si2) or control siRNAs mixed at a ratio of 1:1 in atelocollagen (Koken, Tokyo, Japan) by local injections at 3 and 10 days after subcutaneous tumors had grown to approximately 20 mm^3. We measured the tumor size and calculated the tumor volume. Animal experiments were reviewed and approved by the Institutional Animal Care and Use Committee of our institute.

TUNEL staining of xenografted tumors after treatment

We excised the tumors two days after the last siRNA treatment, fixed them in 10% neutral buffer formalin, and embedded them in paraffin for sectioning and detection of apoptosis. We detected apoptosis by terminal deoxynucleotidyl transferase-mediated deoxyuridine triphosphate biotin nick-end labeling (TUNEL) staining using the ApopTag Plus Peroxidase *In Situ* Apoptosis Detection kit (Chemicon International, Temecula, CA), according to the manufacturer's protocol. Briefly, we stripped nuclear proteins from DNA by incubation in proteinase K for 15 min at room temperature, blocked endogenous peroxidase with 0.3% H_2O_2 for 15 min, and incubated for 10 s with equilibration buffer. The sections were incubated in terminal deoxynucleotidyl transferase enzyme for 1 h at 37 °C. The reaction was terminated by incubation with stop buffer at room temperature. The sections were incubated with anti-digoxigenin conjugate for 30 min, and the reaction was developed with incubation in peroxidase substrate for 5 min. We quantified the TUNEL-stained cells in at least four randomly selected fields at 400× magnification.

Acknowledgments

We thank Sumitaka Hasegawa for technical advices and help, and Yuriko Ogawa for technical assistances. This work was supported in part by a grant from the Ministry of Education, Culture, Sports, Science and Technology of Japan Grant-in Aid for Young Scientists (B) 20790582.

Appendix A. Supplementary data

Supplementary data associated with this article can be found, in the online version, at doi: 10.1016/j.ygeno.2010.02.002.

References

[1] A. Tsiouris, R.K. Walesby, Malignant pleural mesothelioma: current concepts in treatment, Nat. Clin. Pract. Oncol. 4 (2007) 344–352.
[2] B.W. Robinson, R.A. Lake, Advances in malignant mesothelioma, N. Engl. J. Med. 353 (2005) 1591–1603.
[3] N. Kanazawa, A. Ioka, H. Tsukuma, W. Ajiki, A. Oshima, Incidence and survival of mesothelioma in Osaka, Japan, Jpn. J. Clin. Oncol. 36 (2006) 254–257.
[4] J. Peto, A. Decarli, C. La Vecchia, F. Levi, E. Negri, The European mesothelioma epidemic, Br. J. Cancer 79 (1999) 666–672.
[5] K. Berns, et al., A large-scale RNAi screen in human cells identifies new components of the p53 pathway, Nature 428 (2004) 431–437.
[6] J.P. MacKeigan, L.O. Murphy, J. Blenis, Sensitized RNAi screen of human kinases and phosphatases identifies new regulators of apoptosis and chemoresistance, Nat. Cell. Biol. 7 (2005) 591–600.
[7] C.J. Echeverri, N. Perrimon, High-throughput RNAi screening in cultured cells: a user's guide, Nat. Rev. Genet. 7 (2006) 373–384.
[8] A.B. Tsuji, et al., A fast, simple method for screening radiation susceptibility genes by RNA interference, Biochem. Biophys. Res. Commun. 333 (2005) 1370–1377.
[9] H. Sudo, et al., A loss of function screen identifies nine new radiation susceptibility genes, Biochem. Biophys. Res. Commun. 364 (2007) 695–701.
[10] G. Bepler, et al., Characterization of the state of differentiation of six newly established human non-small-cell lung cancer cell lines, Differentiation 37 (1988) 158–171.
[11] A.L. Jackson, et al., Expression profiling reveals off-target gene regulation by RNAi, Nat. Biotechnol. 21 (2003) 635–637.
[12] G.J. Gordon, et al., Identification of novel candidate oncogenes and tumor suppressors in malignant pleural mesothelioma using large-scale transcriptional profiling, Am. J. Pathol. 166 (2005) 1827–1840.
[13] L. Orcl, D.J. Palmer, M. Amherdt, J.E. Rothman, Coated vesicle assembly in the Golgi requires only coatomer and ARF proteins from the cytosol, Nature 364 (1993) 732–734.
[14] J.F. Presley, et al., Dissection of COPI and Arf1 dynamics in vivo and role in Golgi membrane transport, Nature 417 (2002) 187–193.
[15] D. Li, R. Roberts, WD-repeat proteins: structure characteristics, biological function, and their involvement in human diseases, Cell. Mol. Life Sci. 58 (2001) 2085–2097.
[16] K. Hansen, L. Ronnstrand, C. Rorsman, U. Hellman, C.H. Heldin, Association of coatomer proteins with the beta-receptor for platelet-derived growth factor, Biochem. Biophys. Res. Commun. 235 (1997) 455–460.
[17] J.F. Rual, et al., Towards a proteome-scale map of the human protein-protein interaction network, Nature 437 (2005) 1173–1178.
[18] D. Anderson, et al., Binding of SH2 domains of phospholipase C gamma 1, GAP, and Src to activated growth factor receptors, Science 250 (1990) 979–982.

Please cite this article as: H. Sudo, et al., Knockdown of *COPA*, Identified by Loss-of-Function Screen, Induces Apoptosis and Suppresses Tumor Growth in Mesothelioma Mouse Model, Genomics (2010), doi:10.1016/j.ygeno.2010.02.002

Deficiency of the *Erc/mesothelin* gene ameliorates renal carcinogenesis in *Tsc2* knockout mice

Danqing Zhang,[1] Toshiyuki Kobayashi,[1] Tetsuo Kojima,[2] Kenji Kanenishi,[3] Yoshiaki Hagiwara,[1,4] Masaaki Abe,[1] Hidehiro Okura,[1] Yoshitomo Hamano,[1] Guodong Sun,[1] Masahiro Maeda,[4] Kou-ichi Jishage,[5] Tetsuo Noda[6] and Okio Hino[1,7]

[1]Department of Pathology and Oncology, Juntendo University School of Medicine, Tokyo; [2]Chugai Pharmaceutical Co. Ltd, Shizuoka; [3]Department of Perinatology and Gynecology, Kagawa University School of Medicine, Kagawa; [4]Immuno-Biological Laboratories Co. Ltd, Gunma; [5]Chugai Research Institute for Medical Science, Inc., Shizuoka; [6]The JFCR-Cancer Institute, Tokyo, Japan

(Received June 22, 2010/Revised October 14, 2010; December 20, 2010/Accepted December 22, 2010/Accepted manuscript online January 4, 2011)

Genetic crossing experiments were performed between tuberous sclerosis-2 (*Tsc2*) KO and expressed in renal carcinoma (*Erc*) KO mice to analyze the function of the *Erc/mesothelin* gene in renal carcinogenesis. We found the number and size of renal tumors were significantly less in *Tsc2*+/−;*Erc*−/− mice than in *Tsc2*+/−; *Erc*+/+ and *Tsc2*+/−;*Erc*+/− mice. Tumors from *Tsc2*+/−;*Erc*−/− mice exhibited reduced cell proliferation and increased apoptosis, as determined by proliferating cell nuclear antigen (Ki67) and TUNEL analysis, respectively. Adhesion to collagen-coated plates *in vitro* was enhanced in *Erc*-restored cells and decreased in *Erc*-suppressed cells with siRNA. Tumor formation by *Tsc2*-deficient cells in nude mice was remarkably suppressed by stable knockdown of *Erc* with shRNA. Western blot analysis showed that the phosphorylation of focal adhesion kinase, Akt and signal transducer and activator of transcription protein 3 were weaker in *Erc*-deficient/suppressed cells compared with *Erc*-expressed cells. These results indicate that deficiency of the *Erc/mesothelin* gene ameliorates renal carcinogenesis in *Tsc2* KO mice and inhibits the phosphorylation of several kinases of cell adhesion mechanism. This suggests that Erc/mesothelin may have an important role in the promotion and/or maintenance of carcinogenesis by influencing cell-substrate adhesion via the integrin-related signal pathway. (*Cancer Sci*, doi: 10.1111/j.1349-7006.2011.01846.x, 2011)

Expressed in renal carcinoma (*Erc*) was identified as an inducible gene during renal carcinogenesis in the Eker (tuberous sclerosis-2 [*Tsc2*] mutant) rat. The background of this research originates from our studies of the mechanism of multistep carcinogenesis in an animal model involving the *Tsc2* mutant gene using the Eker rat.[1–4] Development of hereditary renal carcinomas in the Eker rat is initiated by a somatic second hit[5] of the *Tsc2* gene. To elucidate the "steps" involved in *Tsc2*-deficiency, genes induced during renal carcinogenesis were cloned in the Eker rat and *Erc* was identified as a novel gene. Subsequently, it was revealed that *Erc* is a homologue of the human *mesothelin* gene.[6] Also, Erc protein is a homologue of a 31-kDa megakaryocyte potentiating factor (MPF), which can stimulate the megakaryocyte colony-forming activity of murine interleukin-3 in mouse bone marrow cell culture. Moreover, Erc protein was also cloned as an antigenic mesothelin for the monoclonal antibody K1 raised against ovarian cancer.[7–9]

Erc/mesothelin protein is a glycosyl phosphatidylinositol (GPI)-anchored membrane glycoprotein that is expressed in normal mesothelial cells. It is also highly expressed in several species of malignant tumors, such as mesothelioma as well as ovarian and pancreatic cancers.[10–13] Its primary product, a 71-kDa precursor of protein, can be physiologically cleaved by a furin-like protease into two fragments. A 31-kDa amino-terminal fragment (MPF, described hereafter as N-Erc/mesothelin) is released into the extra-cellular fluids, while a 40-kDa carboxy-terminal fragment (C-Erc/mesothelin) remains in the cell membranes.[10–16] Soluble N-Erc/mesothelin in serum is already being utilized as a diagnostic tumor marker[14–16] and anti-C-Erc/mesothelin immunotoxin therapy has been reported to be effective for mesothelioma and some C-Erc/mesothelin-expressing cancers.[10] Several *in vitro* studies have suggested that activation of cancer-associated signaling pathways increases Erc/mesothelin expression, and Erc/mesothelin may play a role in tumor adhesion, dissemination, metastasis and resistance against cell death.[9,10,17–22] However, mutant mice in which both copies of the mesothelin gene were inactivated showed no detectable abnormalities when compared with wild-type littermates.[23] Thus, it is conceivable that Erc/mesothelin may have a specific role in carcinogenesis as well as pathogenesis.

The *Erc/mesothelin* gene, described hereafter as *Erc*, is also highly expressed in renal tumor cells from *Tsc2* KO heterozygous mutant (*Tsc2*+/−) mice, that develop hereditary renal tumors presenting as cysts, cyst-adenomas, and solid adenomas that histologically resemble those in the Eker rat.[24]

In this study, *Tsc2*+/−;*Erc*−/− double mutant mice were generated through meiotic recombination and several renal tumor cell lines were established. The phenotypes of the *Tsc2* KO mice with or without *Erc* expression were compared and functions of the *Erc* gene in carcinogenesis were analyzed *in vivo* and *in vitro*. We report here that the development of renal tumors was significantly reduced in *Tsc2*+/−;*Erc*−/− mice, as compared to *Tsc2*+/− (*Erc* WT) or *Tsc2*+/−;*Erc*+/− mice and the several phosphorylation events mediated by integrin and the mammalian target of rapamycin (mTOR) were disrupted in *Tsc2*;*Erc* double deficient renal tumor cells.

Materials and Methods

Gene targeting and generation of *Erc* knockout mouse and crossing with *Tsc2* knockout mouse. Genomic DNA clones covering *Erc* were prepared from a mouse genomic DNA library and used for construction (see Data S1 and Fig. S1 for details).

Tumor measurement and tissue preparation. Mice were sacrificed at 18 months of age. The visible tumors on the renal surface were counted and measured with a caliper for length and width. The size of a tumor was defined to be the tumor's mean diameter: (length [mm] + width [mm])/2. Mice were divided into three groups according to the size of their largest tumor: small (<3 mm), large (3–10 mm) and extra-large (>10 mm). Tissues were fixed in 10% neutral formalin and paraffin sections (3 μm each) were prepared for examination.

[7]To whom correspondence should be addressed. E-mail: ohino@juntendo.ac.jp

doi: 10.1111/j.1349-7006.2011.01846.x

Cell adhesion assay. The assay was performed according to a method described previously[25] with minor modifications and with type I collagen-coated 24-well plates (Iwaki, Tokyo, Japan). Briefly, after blocking nonspecific adhesion with 1% bovine serum albumin in PBS, 1×10^5 cells suspended in 1.0 mL of 10% FCS/RPMI-1640 were added to each well and the cells were allowed to adhere for 1 h at 37°C in a 5% CO_2 incubator. After washing with PBS, the remaining cells were stained with 0.5% crystal violet in 20% methanol for 30 min and then washed away with water. The stained cells were solubilized in 20% acetic acid and the absorbance of the solution was read in a microplate spectrophotometer (Benchmark Plus; Bio-Rad, CA, USA) at 595 nm. Three independent experiments were performed in quadruplicate.

Transplantation assay. BALB/c nude mice were injected subcutaneously with 5×10^6 tumor cells in 100 μL of serum-free medium. After tumors appeared, the tumors were measured weekly with a caliper for length, width and height and the volume was calculated using the following formula: tumor volume (mm^3) = length (mm) × width (mm) × height (mm)/2.

Statistical analysis. All discrete values, expressed as mean ± SEM, were analyzed using Student's *t*-test. *P*-values of <0.05 were considered statistically significant.

See Supporting Information (Data S1) for additional methods.

Results

Establishment of *Tsc2;Erc* double knockout mice. *Trans*-compound double heterozygous mutant (*Tsc2*+/− and *Erc*+/−) male mice were mated with C57BL/6J (WT) females (Fig. 1a). Of the 109 offspring, there was a single mouse carrying both *Tsc2* and *Erc* mutations that is a *cis*-compound double heterozygous mutant (Fig. 1b, white star), provisionally designated Erc109.

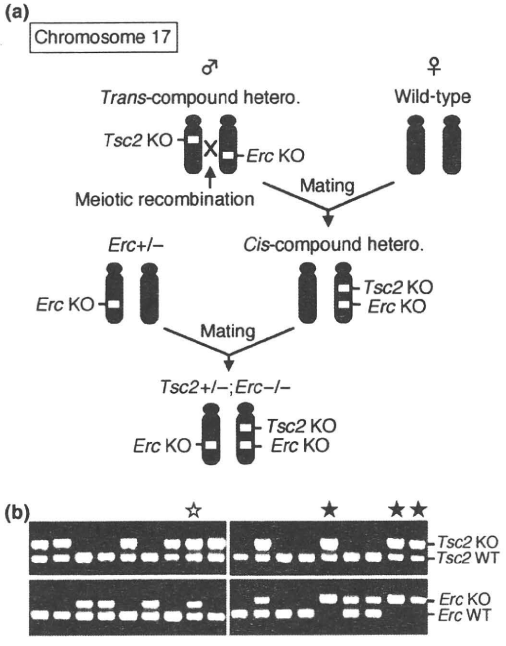

Fig. 1. Generation of tuberous sclerosis-2 (*Tsc2*); expressed in renal carcinoma (*Erc*) double KO mouse. (a) Outline of intercrosses. Only *Erc*-deficient mouse is denoted after second mating. (b) Genotyping of genomic DNA by PCR. Representative results of offspring from first cross (left panels) and second cross (right panels) are shown. Upper and lower panels show genotypes of *Tsc2* and *Erc*, white and black stars indicate the *Tsc2*+/−;*Erc*+/− (*cis*-compound heterozygous) mutant and the *Tsc2*+/−;*Erc*−/− mutant, respectively.

Tsc2+/−;*Erc*−/− mice (Fig. 1b, black stars) were established by mating Erc109 (*Tsc2*+/−;*Erc*+/−) with *Erc* KO mice (Fig. 1a). Absence of Erc protein in *Tsc2*+/−;*Erc*−/− mice was confirmed immunohistochemical staining of the lung mesothelium (Fig. 2a) using anti-mouse C-Erc/mesothelin rabbit polyclonal antibody (Fig. S2).

Reduced renal tumor development in *Tsc2*+/−;*Erc*−/− mice. Renal tumor development was examined in *Tsc2*+/− (*Erc* WT), *Tsc2*+/−;*Erc*+/− and *Tsc2*+/−;*Erc*−/− mice (Fig. 2b–f). Renal tumors were developed in all of the above mice at 18 months of age (Fig. 2b,c,f). However the number (Fig. 2d) and size (mean diameter; Fig. 2b,e,f) of visible tumors on the renal surface were significantly reduced in the *Tsc2*+/−;*Erc*−/− mice. In *Tsc2*+/− as well as *Tsc2*+/−;*Erc*+/− mice, frequent development of tumors of large-size (≥3 mm) were observed in both females and males. There were 59.3% (16 of 27) female and 58.3% (14 of 24) male *Tsc2*+/− mice and 58.6% (17 of 29) female and 57.1% (16 of 28) male *Tsc2*+/−;*Erc*+/− mice that developed large-size tumors. In contrast, only two of 20 females (10.0%) and one of 15 males (6.7%) of *Tsc2*+/−;*Erc*−/− mice showed such large-size tumors (Fig. 2f), although they commonly exhibited carcinogenesis. Moreover, extra-large-size (>10 mm) tumors were seen in *Tsc2*+/− and *Tsc2*+/−;*Erc*+/− mice (11 and 13 cases, respectively) but were not found in *Tsc2*+/−;*Erc*−/− mice (Fig. 2b,f). These observations suggest that the progression of renal tumors in *Tsc2* mutant mice was suppressed by *Erc*-deficiency.

Decreased proliferation in renal tumors from *Tsc2*+/−;*Erc*−/− mice. To elucidate the cellular basis for the effects of *Erc*-deficient on proliferation and apoptosis of renal tumors, the paraffin-embedded renal tumor sections were stained with anti-mouse Ki67 (a proliferating cell nuclear antigen) by immunohistochemistry and TUNEL analysis, respectively (Fig. 3). Tumors derived from *Tsc2*+/−;*Erc*−/− mice not only were significantly reduced tumor cell proliferation (Fig. 3a) but also showed increased apoptosis (Fig. 3b) compared with tumors from *Tsc2*+/−;*Erc*−/− mice although *Erc*-deficient tumors exhibited a mild increase in apoptosis status (Fig. 3c).

Positive effects of Erc on collagen-mediated cell-substrate adhesion in renal tumor cell lines. To conduct an *in vitro* functional analysis of Erc, renal tumor cell lines were established from *Tsc2*+/−;*Erc*−/− mice. Then, *Erc* expression was restored in one of the established cell lines (DE42L-T1-9) by stable transduction of an *Erc* expression vector and the expression of Erc protein was shown by Western blot (Fig. 4a). *Erc*-restored cells (T1-9Ep10 and T1-9Ep13) were found to be more competent to adhere on the collagen-coated plates than *Erc*-deficient (parental and empty-vector) cells (Fig. 4b). To ascertain that the increased adhesion was due to the function of Erc, the expression of Erc in *Erc*-restored cells was re-suppressed by RNAi and the effect of Erc-suppression was verified by RT-PCR and Western blot (Fig. 4c). The adhesion of these cells on collagen-coated plates was significantly reduced by the suppression of *Erc* (Fig. 4d), confirming that Erc positively regulates cell-substrate adhesion.

Suppression of tumorigenesis with *Erc*-suppression in *Tsc2*-deficient renal tumor cells. *Erc*-suppressed cells were established by stable expression of shRNA from the MKOC1-277 cell line that is a *Tsc2*-deficient mouse renal tumor cell line with highly expressed *Erc* (Fig. 5a). When *in vivo* tumorigenicity was examined by subcutaneous injections of cells into nude mice, tumors generated from the *Erc*-suppressed cells were smaller and paler than those from the control shRNA cells that showed robust tumorigenesis (Fig. 5b,c). Conversely, when *Erc*-restored cells were assayed, they exhibited more vigorous growth compared with *Erc*-deficient (empty-vector) cells (Fig. S3). These data suggest that Erc exerts a positive effect on tumorigenicity.

doi: 10.1111/j.1349-7006.2011.01846.x

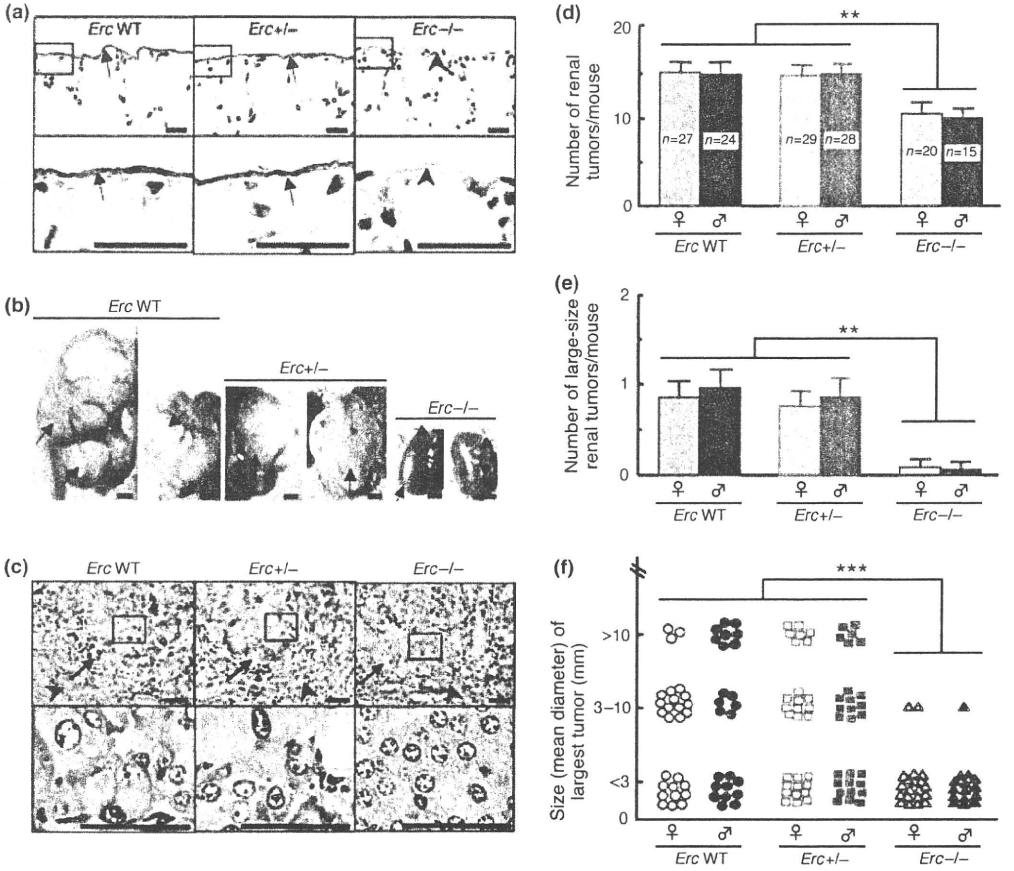

Fig. 2. Reduction of the number and size of renal tumors in expressed in renal carcinoma (*Erc*)-deficient mice. (a) Immunohistochemical staining of anti C-Erc/mesothelin show the positive reactions (arrows) in lung mesothelium of tuberous sclerosis-2 (*Tsc2*)+/– (*Erc* WT) and *Tsc2*+/–;*Erc*+/– mice, but not in *Tsc2*+/–;*Erc*–/– mice (arrowheads). Scale bars = 20 μm. (b) Representative macroscopic findings of the renal tumors (arrows) in 18-month-old mice. Scale bars = 3 mm. (c) H&E staining of sections of renal tumors of above mice. Arrows and arrowheads indicate tumors and normal tissues, respectively. Scale bars = 40 μm. (d) The number of renal tumors was evaluated and expressed as average number per mouse. Values are means ± SEM; $^{**}P < 0.01$. Number of mice measured in each group is shown in columns. (e) The number of large-size (≥3 mm) tumors was selected from (d) and expressed as average number per mouse. Values are means ± SEM; $^{**}P < 0.01$. The number of mice measured in each group is the same as (d). (f) The mice were categorized into three groups according to the size (mean diameter) of the largest tumor that the mouse harbored. Points = the largest tumor of each mouse; $^{***}P < 0.001$. The number of mice measured in each group is the same as (d). The large-size and extra-large-size tumor numbers in the *Erc*–/– mice are significantly less when compared with the other mouse strains.

Modulation of integrin-related signaling by Erc expression. Integrin β1 is a major subunit of collagen receptors[26] and is required for collagen-mediated proliferation of cancer cells.[27–29] Signals from the integrin complex are transmitted through the phosphorylation of focal adhesion kinase (FAK).[30–32] To determine if Erc expression affects cell adhesion through integrin-related signaling, the expression of integrin β1 and the phosphorylated status of downstream molecules were compared among the indicated cell lines (Fig. 6). As previously reported, two major bands were observed in Western blots of integrin β1,[33–37] namely a partially glycosylated 115 kDa precursor and a fully glycosylated 135 kDa mature form. These bands were disappeared or abolished and a band of core peptide (86 kDa) was appeared upon mild (2 μg/mL) tunicamycin (a *N*-glycosylation inhibitor) treatment, confirming the characteristics of integrin β1 (Fig. S4). Mature integrin β1 was dominant in *Erc*-deficient (parental and empty-vector) cells, while the expression of integrin β1 shifted to the precursor in *Erc*-restored cells (Fig. 6a). Reciprocally, levels of the precursor integrin β1 were decreased in *Erc*-suppressed cells compared with *Erc*-expressed (parental and control shRNA) cells (Fig. 6b). Although direct evidence has not yet been obtained, it is plausible that the expression of mature integrin β1 may be regulated by feedback from cell adhesion machinery regulated by Erc.

The level of phosphorylation of FAK (Tyr925) correlated with Erc expression in cells tested (Fig. 6a), suggesting that the signals downstream of integrin are upregulated by Erc. Further tests were conducted for the phosphorylation of Akt (Ser473), S6K (Thr389) and rpS6 (Ser235/236) with three *Tsc2*-related molecules implicated in insulin signaling and mTOR pathway.[38,39] In *Erc*-restored cells, phosphorylation of Akt (Ser473) and rpS6 (Ser235/236) were found to be more robust while phosphorylation of S6K (Thr389) also was induced although to a lesser extent (Fig. 6a). In other words, the phosphorylation of rpS6 (Ser235/236), catalyzed by S6K as is generally known, was shown to be remarkably weaker than S6K (Thr389) in *Erc*-deficient cells and induced in *Erc*-restored cells. The level of phosphorylation of signal transducer and activator of transcription protein 3 (Stat3; Tyr705) is constitutively higher in *Erc*-restored cells than in *Erc*-deficient cells. Positive effects of Erc on these phosphorylated events were also verified in *Erc*-suppressed cells compared with *Erc*-expressing cells (Fig. 6b).

To investigate the molecular basis for the increase in cell adhesion in the *Erc*-restored cells, the cells were treated with

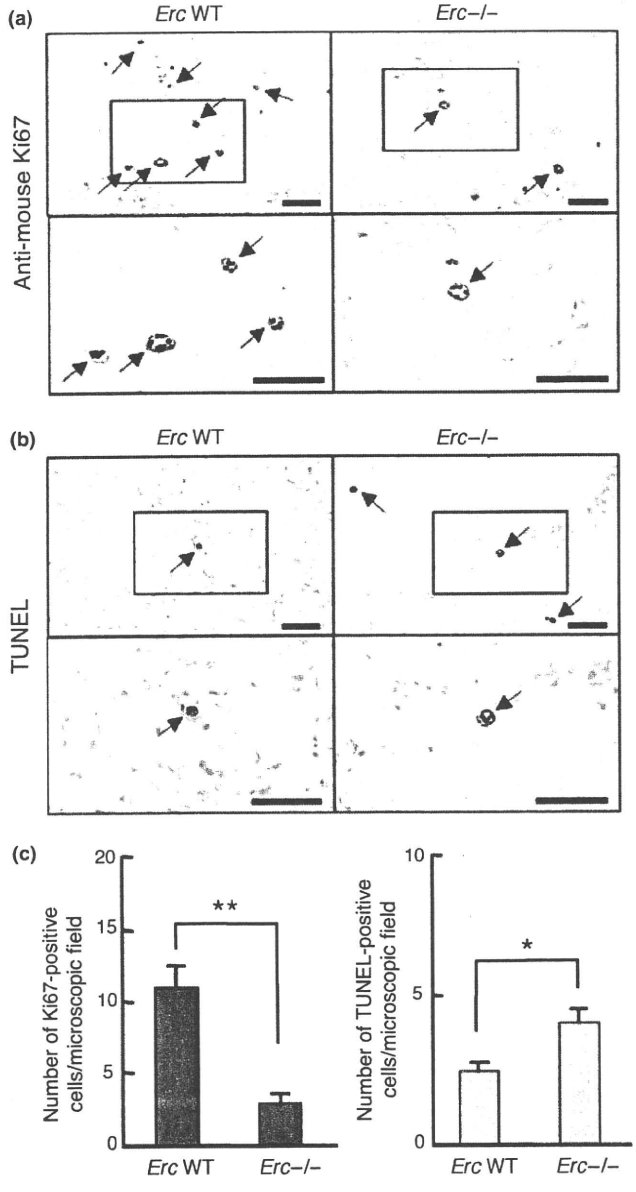

Fig. 3. Expressed in renal carcinoma (*Erc*)-deficient decreases tumor growth by impairing cell proliferation. (a) Proliferation was assessed by immunohistochemistry staining on sections of paraffin-embedded renal tumors of the indicated genotype with Ki67 antibody. Positive cells appear brown (arrows). Scale bars = 40 μm. (b) TUNEL-stained sections of paraffin-embedded renal tumors of the indicated genotype. Apoptotic cells appear brown (arrows). Scale bars = 40 μm. (c) The number of Ki67-positive cells (left panel) or TUNEL-positive cells (right panel) per microscopic field was evaluated as described in the Data S1. Values are means (n = 30 images per genotype) ± SEM; $^{**}P < 0.01$; $^{*}P < 0.05$.

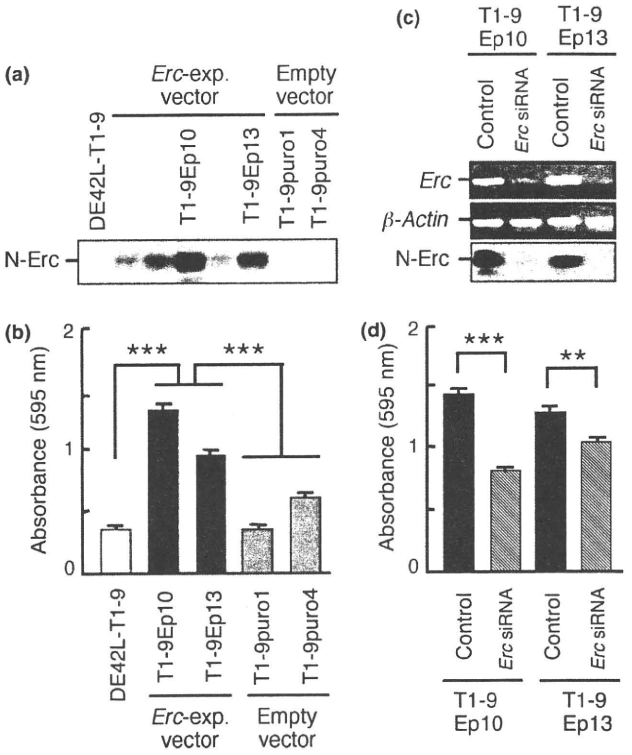

Fig. 4. Expressed in renal carcinoma (*Erc*)-expression enhanced cell adhesion to collagen-coated plates. (a) Western blot analysis showed the level of N-Erc expression in the cell lines used for cell adhesion assay. Name of each cell used for further analysis is shown. (b) The adhesion was enhanced in stable *Erc*-restored cells (T1-9Ep10 and T1-9EP13) compared with *Erc*-deficient parental cell line (DE42L-T1-9) and empty-vector cells (T1-9puro1 and T1-9puro4). Values are means ± SEM; $^{***}P < 0.001$. Three independent experiments were performed in quadruplicate. (c) RT-PCR (*Erc* and *β-Actin*) and Western blot analysis (N-Erc) showed the effects of *Erc*-suppression when treated with *Erc* siRNA in *Erc*-restored cells. (d) In contrast to results in (b), the adhesion was decreased in *Erc*-restored cells treated with siRNA. Values are means ± SEM; $^{***}P < 0.001$; $^{**}P < 0.01$. Three independent experiments were performed in quadruplicate.

DMSO (control), 10 μM Akt-I-1/2 (an Akt inhibitor) or 0.1 μM wortmannin (a phosphatidylinositol-3-OH kinase [PI3K] inhibitor), respectively, and then measured the activation of the Akt and the cell adhesion. As shown in Figure 7a, the phosphorylation of Akt (Ser473) was suppressed completely but the phosphorylation of FAK (Tyr925) was not affected in the cells that were treated with an Akt-I-1/2 or wortmannin. The cell adhesion to collagen-coated plates was remarkably decreased in *Erc*-restored cell (T1-9Ep10) treated by both inhibitors compared with control (DMSO) cells (Fig. 7b). These suggest that the activation of Akt by Erc is dependent on PI3K and the cell adhesion positively regulated by PI3K-Akt pathway because phosphorylation of FAK was not affected by Akt-inhibitor or PI3K-inhibitor treatment.

Discussion

The *Erc* gene is highly expressed in renal tumor cells compared to normal renal cells of *Tsc2*+/− KO mice. Our newly generated *Tsc2*;*Erc* double KO mice made it feasible to investigate the function of Erc in carcinogenesis in a mouse tumor model. The results clearly showed that deficiency of Erc decreased the number and size of renal tumors, and reduced cell proliferation and increased apoptosis in *Tsc2* KO mice, inhibited cell adhesion to collagen-coated plates, and suppressed tumor formation in nude mice. We also showed that Erc influenced the expression of integrin β1 and phosphorylation of several downstream proteins, such as FAK, Akt, rpS6 and Stat3.

The *Tsc2* KO mice and Eker rats, both of which are *Tsc2* heterozygous mutants, develop renal tumors through loss of *Tsc2* in

doi: 10.1111/j.1349-7006.2011.01846.x

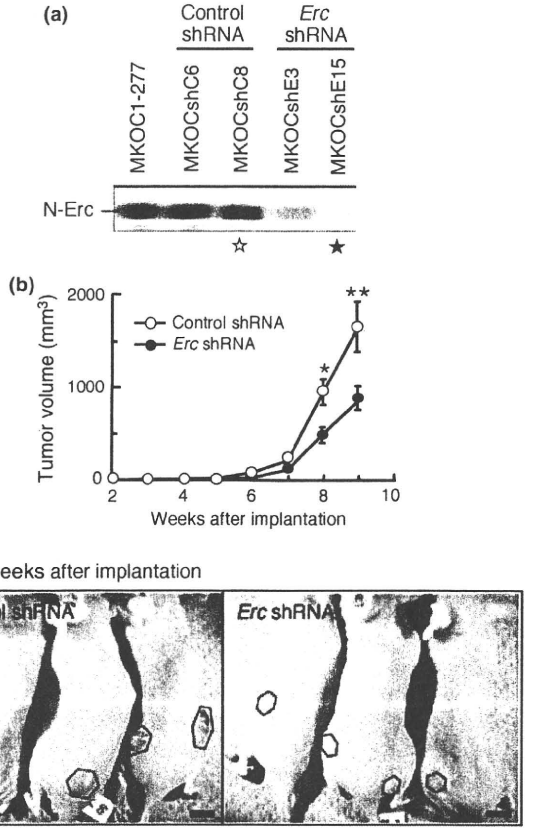

Fig. 5. Expressed in renal carcinoma (*Erc*)-deficiency suppressed tumorigenicity of renal tumor cells transplanted in nude mice. (a) Western blot analysis showed the level of N-Erc expression in the stable *Erc*-suppressed cell lines. Black and white stars indicate the cells used for tumorigenicity assay shown below. (b) The tumor volumes were suppressed in stable *Erc*-suppressed (MKOCshE15, black circles) cells compared with control-shRNA (MKOCshC8, white circles) cells after implantation into nude mice. Values are means ± SEM (n = 6); $^{**}P < 0.01$; $^{*}P < 0.05$. (c) Macroscopic appearance of tumors was shown at 8 weeks after implantation. Tumor areas are marked with hexagons. Scale bars = 10 mm.

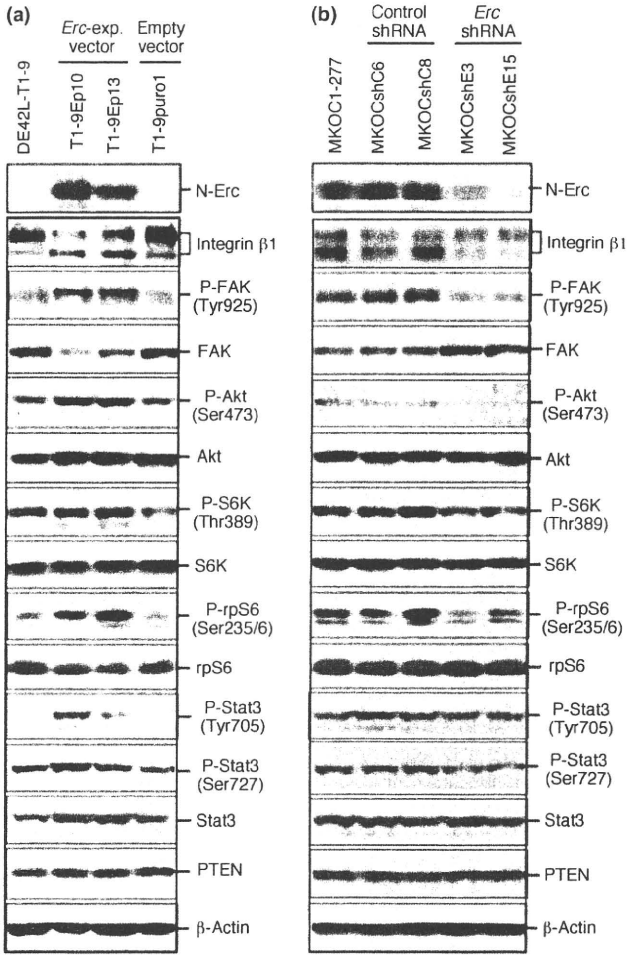

Fig. 6. Expressed in renal carcinoma (*Erc*) expression affects integrin-related signal. Western blot analysis was performed with indicated antibodies; the concentrated culture supernatant lysates were used for N-Erc and whole-cell lysates were used for other antibodies. (a) The stable *Erc*-restored cells (central two lanes) increased the precursor integrin β1 (lower-band) and the level of phosphorylation of focal adhesion kinase (FAK), Akt, S6K, rpS6 and Stat3 compared with *Erc*-deficient parental cell line (left lane) and the empty-vector cell (right lane). (b) The stable *Erc*-suppressed cells (right two lanes) decreased the precursor integrin β1 (lower-band) and the level of phosphorylation of FAK, Akt, S6K, rpS6 and Stat3 compared with *Erc*-express (WT) parental cell line (left lane) and the control-shRNA cells (central two lanes).

the WT allele and in multi-steps.[1–5] The human TSC disease is caused by germ-line mutations in either the *TSC1* or *TSC2* gene, with numerous individual tumors generally arising due to somatic ''second-hit'' mutations or loss of heterozygosity[24,40] similar to the above animal models. The resulting tumors in humans and in animal models display elevated mTOR signaling, leading to the enhanced phosphorylation of S6K and rpS6.[1–4,41,42] Erc is highly expressed in renal tumor cells of Eker rats and *Tsc2* KO mice[6,24] but the state of Erc has not been reported in human TSC disease.

The mTOR pathway has a pivotal function in the coordination of cell metabolism, cell growth and cell proliferation[40–44] but another pathway may be involved in *Tsc2* mutant animal models. It has been reported that the administration of rapamycin alone to *Tsc2*-mutant animal models (KO mice and Eker rats) with established tumors results in tumor regression. This however, is characterized with residual tumor or failure to eradicate microscopic pre-tumorous lesions.[45–47] These results suggested the existence of other pathways involved in the *Tsc2*-mutant, in addition to the mTOR axis. The *Tsc2*;*Erc* double KO mice exploited here allowed us to investigate this putative pathway without the confounding effects of possible drug resistance. Our results strongly supported the existence of another pathway, in addition to the mTOR axis.

Recently, it was reported that hotspots of GPI-anchored proteins and integrin nanoclusters were involved in cell adhesion.[48] This was corroborated by our results that showed the expression of Erc affected the pattern of integrin and phosphorylation of several kinases because Erc is one of the GPI-anchored proteins. The new pathway displaying an Erc-cell adhesion mediated tumor-proliferation function may exist, but no association between Erc and integrin-related signal has been reported. Although Erc expression is associated with the decrease in the amount of mature integrin β1, this phenomenon may be caused by some feedback mechanism from activated cell-adhesion machinery partially regulated by Erc.

Signals from the integrin complex are transmitted through the phosphorylation of FAK.[30–32] Akt is a *Tsc2*-related molecule

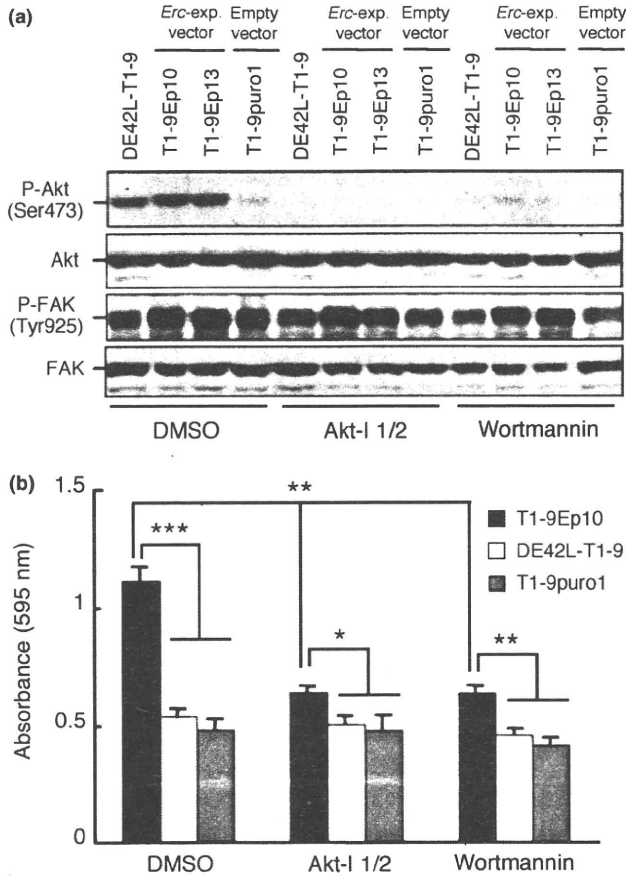

Fig. 7. Cell adhesion was decreased by treated with an Akt inhibitor and a PI3K inhibitor. The cells which are the same as Figure 6a, were divided into three groups and treated with DMSO (control), 10 μM Akt-I-1/2 (an Akt inhibitor) or 0.1 μM wortmannin (a PI3K inhibitor), respectively. (a) Western blot analysis was performed with indicated antibodies. The phosphorylation of Akt (Ser473) was suppressed completely with both the inhibitors but the phosphorylation of focal adhesion kinase (FAK; Tyr925) was not affected. (b) The cell adhesion to collagen-coated plates was remarkably decreased in *Erc*-restored cell treated by both inhibitors compared with control (DMSO) cells. Values are means ± SEM; $***P < 0.001$, $*P < 0.01$, $*P < 0.05$. Three independent experiments were performed in quadruplicate.

implicated in insulin signaling[38,39] known to be activated by cell adhesion-related signaling.[49] Our results showed that the level of phosphorylation of FAK (Tyr925), Akt (Ser473) and rpS6 (Ser235/236) were decreased with *E*rc-deficient cells (both *E*rc KO and *E*rc knock down) while the phosphorylation of S6K (Thr389) was reduced to a lesser extent, suggesting that integrin signaling and downstream proteins were upregulated by Erc.

It is well known that *Tsc2*-deficiency activates the mTORC1-S6K pathway as well as the downregulation of Akt.[50] However, our results showed the further downregulation of phosphorylation of Akt (Ser473) by *Erc*-deficiency in *Tsc2*-deficient cells and upregulation in *E*rc-restored cells *in vitro*, suggesting that *Erc*-deficiency is relevant to the suppression of tumor development in *Tsc2*+/− mice. The function of Erc might support the receptor signaling through the cell adhesion signaling. Deficiencies of *Tsc2* and *Erc* might be co-operatively involved in tumorigenesis in KO mice.

The important role of *Erc* in carcinogenesis has attracted a great deal of attention in recent years.[6–22] Several authors reported that overexpression of Erc can accelerate the proliferation and adhesion of cancer cells using cell lines and xenograft models of cancer.[9,10,17–22] Our previous study showed that *Erc* gene expression silenced by siRNA suppresses tumor growth in the *Tsc2* mutant renal carcinoma model.[51] The activation of specific signaling pathways that are important in cancer can lead to an increase in Erc expression. Binding of ovarian cancer antigen CA125/MUC16 to Erc mediates cell adhesion.[17] The overexpression of Erc in pancreatic cancer cells leads to constitutive activation of the transcription factor Stat3, which results in enhanced expression of cyclin E and cyclin E/cyclin-dependent kinase 2 complex formation, as well as increased G1-S transition.[20] Erc inhibits paclitaxel-induced apoptosis through the PI3K pathway.[21] Erc is also differentially regulated by members of the Wnt signal transduction pathway.[22] Combining these reports with our data, multiple possibilities can be considered. First, the pathological high-expression of Erc in specific malignant tumors of humans and in animal models is considered to be the result of carcinogenesis by the mutant *Tsc2* or other key gene. The pathological high-expression of Erc plays a prominent role in many signal transduction pathways such as CA125/MUC16, Stat3, PI3K and Wnt, although elucidation of the underlying mechanism remains elusive. Second, since mutant mice in which both copies of the Erc gene were inactivated showed no detectable abnormalities as compared to WT littermates,[23] Erc might have a function specific to carcinogenesis and other pathological conditions. Third, the downregulation of an integrin-related pathway may affect the progression of multi-step carcinogenesis and inhibit the development of large tumors in *Tsc2*+/−;*Erc*−/− mice.

In conclusion, we report here that deficiency of Erc affected the integrin-related signal pathway and suppressed the growth of renal tumors in *Tsc2* KO mice. An understanding of the signaling pathways and mechanisms of Erc-induced tumor cell adhesion, proliferation and survival may elucidate not only the pathogenesis of renal tumors in Tsc2+/− mice, but also the pathogenesis of other malignant tumors in both animal models and humans. Our experimental system of *Tsc*;*Erc* KO mice and cells is useful to unravel the important role of Erc during carcinogenesis, and further analysis of the Erc pathway may help to develop novel anti-cancer therapies.

Acknowledgments

We thank Nobuo Kamada, Miho Watanabe and Yousuke Kawase (Chugai Research Institute for Medical Science, Inc., Shizuoka, Japan) for mouse production; Youko Hirayama, Hiroaki Mitani, Junko Sakurai (The JFCR-Cancer Institute, Tokyo, Japan), Etsuko Kobayashi, Norihiro Tada, Fumio Kanai, Keiichi Sasahara, Naomi Ohtsuji and Tetsuya Takagaki (Juntendo University School of Medicine, Tokyo, Japan), for technical assistance; Kazunori Kajino, Shuji Momose, Shuji Matsuoka, Xianghua Piao and other members of the Hino laboratory for helpful discussions. This works was supported by a Grant-in-Aid for Cancer Research from the Ministry of Education, Science, Technology, Sports and Culture, Japan, and Grants-in-Aid for Scientific Research from Japan Society for the Promotion of Science, and the Ministry of Health, Labour and Welfare, Japan.

doi: 10.1111/j.1349-7006.2011.01846.x

References

1 Eker R, Mossige J. A dominant gene for renal adenomas in the rat. *Nature* 1961; **189**: 858–9.
2 Hino O, Kobayashi T, Momose S, Kikuchi Y, Adachi H, Okimoto K. Renal carcinogenesis: genotype, phenotype and dramatype. *Cancer Sci* 2003; **94**: 142–7.
3 Hino O, Kobayashi T, Tsuchiya H *et al.* The predisposing gene of the Eker rat inherited cancer syndrome is tightly linked to the tuberous sclerosis (TSC2) gene. *Biochem Biophys Res Commun* 1994; **203**: 1302–8.
4 Kobayashi T, Hirayama Y, Kobayashi E, Kubo Y, Hino O. A germline insertion in the tuberous sclerosis (*Tsc2*) gene gives rise to the Eker rat model of dominantly inherited cancer. *Nat Genet* 1995; **9**: 70–4.
5 Knudson AG. Mutation and cancer: statistical study of retinoblastoma. *Proc Natl Acad Sci U S A* 1971; **68**: 820–3.
6 Hino O, Kobayashi E, Nishizawa M *et al.* Renal carcinogenesis in the Eker rat. *J Cancer Res Clin Oncol* 1995; **121**: 602–5.
7 Kojima T, Oh-eda M, Hattori K *et al.* Molecular cloning and expression of megakaryocyte potentiating factor cDNA. *J Biol Chem* 1995; **270**: 21984–90.
8 Chang K, Pastan I. Molecular cloning of mesothelin, a differentiation antigen present on mesothelium, mesotheliomas, and ovarian cancers. *Proc Natl Acad Sci U S A* 1996; **93**: 136–40.
9 Yamashita Y, Yokoyama M, Kobayashi E, Takai S, Hino O. Mapping and determination of the cDNA sequence of the *Erc* gene preferentially expressed in renal cell carcinoma in the *Tsc2* gene mutant (Eker) rat model. *Biochem Biophys Res Commun* 2000; **275**: 134–40.
10 Hassan R, Bera T, Pastan I. Mesothelin: a new target for immunotherapy. *Clin Cancer Res* 2004; **10**: 3937–42.
11 Scholler N, Fu N, Yang Y *et al.* Soluble member(s) of the mesothelin/megakaryocyte potentiating factor family are detectable in sera from patients with ovarian carcinoma. *Proc Natl Acad Sci U S A* 1999; **96**: 11531–6.
12 Sapede C, Gauvrit A, Barbieux I *et al.* Aberrant splicing and protease involvement in mesothelin release from epithelioid mesothelioma cells. *Cancer Sci* 2008; **99**: 590–4.
13 Li M, Bharadwaj U, Zhang R *et al.* Mesothelin is a malignant factor and therapeutic vaccine target for pancreatic cancer. *Mol Cancer Ther* 2008; **7**: 286–96.
14 Robinson BW, Creaney J, Lake R *et al.* Mesothelin-family proteins and diagnosis of mesothelioma. *Lancet* 2003; **362**: 1612–6.
15 Hino O, Maeda M. Diagnostic tumor marker of asbestos-related mesothelioma. *Environ Health Prev Med* 2008; **13**: 71–4.
16 Shiomi K, Hagiwara Y, Sonoue K *et al.* Sensitive and specific new enzyme-linked immunosorbent assay for N-ERC/mesothelin increases its potential as a useful serum tumor marker for mesothelioma. *Clin Cancer Res* 2008; **14**: 1431–7.
17 Rump A, Morikawa Y, Tanaka M *et al.* Binding of ovarian cancer antigen CA125/MUC16 to mesothelin mediates cell adhesion. *J Biol Chem* 2004; **279**: 9190–8.
18 Hucl T, Brody JR, Gallmeier E, Iacobuzio-Donahue CA, Farrance IK, Kern SE. High cancer-specific expression of mesothelin (MSLN) is attributable to an upstream enhancer containing a transcription enhancer factor dependent MCAT motif. *Cancer Res* 2007; **67**: 9055–65.
19 Que J, Wilm B, Hasegawa H, Wang F, Bader D, Hogan BL. Mesothelium contributes to vascular smooth muscle and mesenchyme during lung development. *Proc Natl Acad Sci U S A* 2008; **105**: 16626–30.
20 Bharadwaj U, Li M, Chen C, Yao Q. Mesothelin-induced pancreatic cancer cell proliferation involves alteration of cyclin E via activation of signal transducer and activator of transcription protein 3. *Mol Cancer Res* 2008; **6**: 1755–65.
21 Chang MC, Chen CA, Hsieh CY *et al.* Mesothelin inhibits paclitaxel-induced apoptosis through the PI3K pathway. *Biochem J* 2009; **424**: 449–58.
22 Prieve MG, Moon RT. Stromelysin-1 and mesothelin are differentially regulated by Wnt-5a and Wnt-1 in C57MG mouse mammary epithelial cells. *BMC Dev Biol* 2003; **3**: 2–11.
23 Bera TK, Pastan I. Mesothelin is not required for normal mouse development or reproduction. *Mol Cell Biol* 2000; **20**: 2902–6.
24 Kobayashi T, Minowa O, Kuno J, Mitani H, Hino O, Noda T. Renal carcinogenesis, hepatic hemangiomatosis, and embryonic lethality caused by a germ-line *Tsc2* mutation in mice. *Cancer Res* 1999; **59**: 1206–11.
25 Gustavsson A, Armulik A, Brakebusch C, Fässler R, Johansson S, Fällman M. Role of the β1-integrin cytoplasmic tail in mediating invasin-promoted internalization of Yersinia. *J Cell Sci* 2002; **115**: 2669–78.
26 Harburger DS, Calderwood DA. Integrin signalling at a glance. *J Cell Sci* 2009; **122**: 159–63.
27 Macias-Perez I, Borza C, Chen X *et al.* Loss of integrin α1 β1 ameliorates Kras-induced lung cancer. *Cancer Res* 2008; **68**: 6127–35.
28 Brenner W, Greber I, Gudejko-Thiel J *et al.* Migration of renal carcinoma cells is dependent on protein kinase Cdelta via beta1 integrin and focal adhesion kinase. *Int J Oncol* 2008; **32**: 1125–31.
29 Park CC, Zhang H, Pallavicini M *et al.* Beta1 integrin inhibitory antibody induces apoptosis of breast cancer cells, inhibits growth, and distinguishes malignant from normal phenotype in three dimensional cultures and in vivo. *Cancer Res* 2006; **66**: 1526–35.
30 Shibue T, Weinberg RA. Integrin β1-focal adhesion kinase signaling directs the proliferation of metastatic cancer cells disseminated in the lungs. *Proc Natl Acad Sci U S A* 2009; **106**: 10290–5.
31 Xia H, Nho RS, Kahm J, Kleidon J, Henke CA. Focal adhesion kinase is upstream of phosphatidylinositol 3-kinase/Akt in regulating fibroblast survival in response to contraction of type I collagen matrices via a beta 1 integrin viability signaling pathway. *J Biol Chem* 2004; **279**: 33024–34.
32 Pylayeva Y, Gillen KM, Gerald W, Beggs HE, Reichardt LF, Giancotti FG. Ras- and PI3K-dependent breast tumorigenesis in mice and humans requires focal adhesion kinase signaling. *J Clin Invest* 2009; **119**: 252–66.
33 Argraves WS, Suzuki S, Arai H, Thompson K, Pierschbacher MD, Ruoslahti E. Amino acid sequence of the human fibronectin receptor. *J Cell Biol* 1987; **105**: 1183–90.
34 Guo HB, Lee I, Kamar M, Akiyama SK, Pierce M. Aberrant *N*-glycosylation of beta1 integrin causes reduced alpha5beta1 integrin clustering and stimulates cell migration. *Cancer Res* 2002; **62**: 6837–45.
35 Bellis SL, Newman E, Friedman EA. Steps in integrin beta1-chain glycosylation mediated by TGFbeta1 signaling through Ras. *J Cell Physiol* 1999; **181**: 33–44.
36 Isaji T, Sato Y, Fukuda T, Gu J. *N*-glycosylation of the I-like domain of beta1 integrin is essential for beta1 integrin expression and biological function: identification of the minimal *N*-glycosylation requirement for alpha5beta1. *J Biol Chem* 2009; **284**: 12207–16.
37 Bellis SL. Variant glycosylation: an underappreciated regulatory mechanism for beta1 integrins. *Biochim Biophys Acta* 2004; **1663**: 52–60. Review.
38 Inoki K, Corradetti MN, Guan KL. Dysregulation of the TSC-mTOR pathway in human disease. *Nat Genet* 2005; **37**: 19–24.
39 Cao Y, Kamioka Y, Yokoi N *et al.* Interaction of FoxO1 and TSC2 induces insulin resistance through activation of the mammalian target of rapamycin/p70 S6K pathway. *J Biol Chem* 2006; **281**: 40242–51.
40 Astrinidis A, Henske EP. Tuberous sclerosis complex: linking growth and energy signaling pathways with human disease. *Oncogene* 2005; **24**: 7475–81.
41 Kobayashi T, Adachi H, Mitani H, Hirayama Y, Hino O. Toward chemotherapy for *Tsc2 mutant* renal tumor. *Proc Jpn Acad* 2003; **79**: 22–5.
42 Shiono M, Kobayashi T, Takahashi R *et al.* The G1556S-type tuberin variant suppresses tumor formation in tuberous sclerosis 2 mutant (Eker) rats despite its deficiency in mTOR inhibition. *Oncogene* 2008; **27**: 6690–7.
43 Guertin DA, Sabatini DM. Defining the role of mTOR in cancer. *Cancer Cell* 2007; **12**: 9–22.
44 Gan B, Yoo Y, Guan J-L. Association of focal adhesion kinase with tuberous sclerosis complex 2 in the regulation of s6 kinase activation and cell growth. *J Biol Chem* 2006; **281**: 37321–9.
45 Kenerson H, Dundon TA, Yeung RS. Effects of rapamycin in the Eker rat model of tuberous sclerosis complex. *Pediatr Res* 2005; **57**: 67–75.
46 Lee L, Sudentas P, Donohue B *et al.* Efficacy of a rapamycin analog (CCI-779) and IFN-gamma in tuberous sclerosis mouse models. *Genes Chromosomes Cancer* 2005; **42**: 213–27.
47 Lee L, Sudentas P, Dabora SL. Combination of a rapamycin analog (CCI-779) and interferon-gamma is more effective than single agents in treating a mouse model of tuberous sclerosis complex. *Genes Chromosomes Cancer* 2006; **45**: 933–44.
48 van Zanten TS, Cambi A, Koopman M *et al.* Hotspots of GPI-anchored proteins and integrin nanoclusters function as nucleation sites for cell adhesion. *Proc Natl Acad Sci U S A* 2009; **106**: 18557–62.
49 Barros CS, Nguyen T, Spencer KS, Nishiyama A, Colognato H, Müller U. β1 integrins are required for normal CNS myelination and promote AKT-dependent myelin outgrowth. *Development* 2009; **136**: 2717–24.
50 Huang J, Wu S, Wu CL, Manning BD. Signaling events downstream of mammalian target of rapamycin complex 2 are attenuated in cells and tumors deficient for the tuberous sclerosis complex tumor suppressors. *Cancer Res* 2009; **69**: 6107–14.
51 Imamura O, Okada H, Takashima Y, Zhang D, Kobayashi T, Hino O. siRNA-mediated Erc gene silencing suppresses tumor growth in Tsc2 mutant renal carcinoma model. *Cancer Lett* 2008; **268**: 278–85.

Supporting Information

Additional Supporting Information may be found in the online version of this article:

Data S1. Supporting Methods.

Fig. S1. Establishment of expressed in renal carcinoma (*Erc*) KO mice.

Fig. S2. Amino acid alignment of the expressed in renal carcinoma (Erc)/mesothelin protein.

Fig. S3. Enhanced tumorigenicity of expressed in renal carcinoma (*Erc*)-restored renal tumor cells transplanted in nude mice.

Fig. S4. Confirmed the characteristics of integrin β1 by treated with lower concentration of tunicamycin.

doi: 10.1111/j.1349-7006.2011.01846.x

Journal of Crystal Growth 312 (2010) 2764–2770

Contents lists available at ScienceDirect

Journal of Crystal Growth

journal homepage: www.elsevier.com/locate/jcrysgro

The effect of solvent ratio and water on the growth of C_{60} nanowhiskers

Kun'ichi Miyazawa*, Kayoko Hotta

Fullerene Engineering Group, Exploratory Nanotechnology Research Laboratory, National Institute for Materials Science, 1-1 Namiki, Tsukuba, Ibaraki 305-0044, Japan

ARTICLE INFO

Article history:
Received 23 April 2010
Received in revised form
12 June 2010
Accepted 14 June 2010
Available online 17 June 2010

Keywords:
A1. Liquid–liquid interfacial precipitation method (LLIP)
B1. Fullerene nanowhiskers
B1. C_{60} nanowhiskers
B1. Fullerene

ABSTRACT

The growth of C_{60} nanowhiskers (C_{60}NWs) prepared by a modified liquid–liquid interfacial precipitation method is investigated, focusing on the effect of solvent ratio and water content in the C_{60}–toluene–isopropyl alcohol (IPA) solution system. The precipitation of C_{60}NWs was markedly influenced by the solvent ratio of toluene to IPA, and the C_{60}NWs were found to grow longer above a critical diameter (D_c), which depends on the solvent ratio. The addition of a small amount of H_2O to the C_{60}–toluene–IPA solution promoted the growth of C_{60}NWs. This catalytic effect of water on the growth of C_{60}NWs was confirmed also by the experiment using heavy water (D_2O) and by the decrease of growth activation energy of C_{60}NWs with increase of H_2O content in the C_{60}–toluene–IPA solution.

1. Introduction

C_{60} nanowhiskers (C_{60}NWs) are thin single crystal nanofibers composed of C_{60} molecules [1]. In 2001, C_{60}NWs were found to precipitate in a colloidal solution of lead zirconate titanate (PZT) containing a small amount of C_{60} [2]. In addition to the C_{60}NWs, various kinds of fullerene nanowhiskers (FNWs) that are composed of C_{70}, $C_{60}[C(COOC_2H_5)_2]$, La@C_{82}(Ad) (Ad= adamantylidene) and so forth have been synthesized using the liquid–liquid interfacial precipitation method (LLIP method) [3–5]. Single crystal tubular nanofibers composed of C_{70}, "C_{70} nanotubes" [6], were also synthesized by the LLIP method as well as C_{60} nanotubes [7,8].

The LLIP method uses the interdiffusion process between a good solvent solution of fullerene and a poor solvent of fullerene after placing the good solvent solution of fullerene on the poor solvent to precipitate the FNWs [3,9]. The interdiffusion occurs by self-diffusion [3] or can be assisted by manual mixing or ultrasonication [10–12]. The LLIP method without the process of manual mixing or ultrasonication is called the "static LLIP method" in this paper.

Not only long fibrous C_{60}NWs with lengths greater than several millimeters [13] but also short C_{60}NWs with lengths from several micrometers to several tens of micrometers can be prepared by the LLIP method [10,14–16].

Cha et al. [17] fabricated vertically grown C_{60} microtubes on a porous alumina membrane substrate by slowly injecting IPA through the membrane pores into a C_{60}-saturated toluene solution in order to induce supersaturation of C_{60} on the membrane surface. Further, Cha et al. [18] fabricated tree-shaped bundled C_{60}NWs by injecting IPA into a toluene solution of C_{60} containing the ferrocene derivative of C_{60} molecules through a porous alumina membrane. Recently Sathish et al. [19] and Satish and Miyazawa [20] fabricated various morphologies of fine C_{60} crystals containing C_{60} nanosheets, short C_{60}NWs with lengths between a few micrometers and several micrometers and nanorhombuses of C_{60} by the LLIP method. Slightly later Masuhara et al. [21] also reported the production of various morphologies of spherical particles, whiskers, hexagonal plates, nanoballs and nanobipyramids of C_{60}, where good solvent solutions of C_{60} were injected into poor solvents of C_{60}.

C_{60}NWs exhibit semiconductor properties [22,23], and were first applied to field-effect transistors [24]. Various other applications of C_{60}NWs are expected in catalysts [1,25–28], fuel cells [29,30], solar cells [31], and so forth.

As shown in our earlier paper [4], C_{60}NWs with diameters less than 100 nm can be synthesized by the static LLIP method. Fibrous C_{60}NWs with a small diameter of 87 nm and a length of more than 5 μm were produced. Afterward, Chong et al. [32] studied the fabrication of C_{60}NWs by dropping a toluene solution of C_{60} into IPA to precipitate C_{60} crystals and reported a needle-like crystal of C_{60} with a diameter of about 80 nm and a length of about 500 nm for an example of "true nanoscale single crystal of C_{60}". The fabrication of nanoscale C_{60} single crystal was also demonstrated by the formation of a needle-like crystal with a small diameter of 45 nm and a length of 108 nm by dropping a C_{60}-saturated toluene solution into IPA under ultrasonication at 10 °C [11].

* Corresponding author. Tel.: +81 29 860 4528; fax: +81 29 860 4667.
E-mail address: miyazawa.kunichi@nims.go.jp (K. Miyazawa).

0022-0248/$ - see front matter © 2010 Elsevier B.V. All rights reserved.
doi:10.1016/j.jcrysgro.2010.06.020

As shown above, a variety of methods derived from the static LLIP method have been used to synthesize C_{60}NWs of various lengths and diameters. The size control of C_{60}NWs is important in their practical application. For example, short C_{60}NWs with lengths of several micrometers are appropriate for solar cell application [31], while long C_{60}NWs are appropriate when they are used to fabricate non-woven sheets of C_{60} [33]. C_{60}NWs with small sizes will be required for their application to transistors.

In order to control the size of C_{60}NWs, the growth mechanism of C_{60}NWs must be clear. Up to now, the following items have been reported:

(1) Growth of C_{60}NWs is promoted by illumination of visible light and depends on the wavelength of light [34,35].
(2) Growth of C_{60}NWs depends on temperature. The growth activation energy of C_{60}NWs was measured to be 52.8 kJ/mol in the system of C_{60}-saturated toluene solution and IPA [15].
(3) Growth of C_{60}NWs is promoted by addition of a small amount of water [36].
(4) Morphology of precipitated C_{60} crystals depends on the solvent ratio of toluene to IPA and the amount of added water [36].

We partly reported the effects of water and solvent ratio on morphology and growth of C_{60}NWs in our preliminary experiments [36]. Hence in the present paper, the above items (2)–(4) are more minutely investigated and the effects of solvent ratio and water on growth of C_{60}NWs are discussed in detail.

The results shown below must be useful for growth control of C_{60}NWs and will also be informative in the synthesis of fullerene nanowhiskers using the solvent combinations different from toluene and IPA as well.

2. Experimental

2.1. Synthesis of C_{60}NWs using different solvent ratios

In preparing C_{60}NWs, toluene (99.5% purity, as-received non-dehydrated grade, Wako Pure Chemical Industries, Ltd., Japan) was used as a good solvent of C_{60} and IPA (as-received non-dehydrated grade, Wako Pure Chemical Industries, Ltd., Japan) was used as a poor solvent of C_{60}. The water content of the as-received IPA was measured to be 0.02% and that of the as-received toluene was measured to be 0.01% using a Karl Fischer titrator (Coulometer 831 KF). Ground C_{60} powder (99.5% purity, MTR Ltd., USA) was dissolved in toluene by ultrasonication for 30 min and filtered to remove the undissolved C_{60} powder.

C_{60}NWs were prepared by a modified LLIP method as follows. The C_{60}-saturated toluene solution was poured into a 10 ml transparent glass bottle and IPA was slowly added to the C_{60}-saturated toluene solution to form a liquid–liquid interface in a water bath at 20 °C. Next, the glass bottles were manually shaken 30 times in order to obtain homogeneous precipitation of embryo crystals of C_{60} and kept in an incubator (SANYO MIR-153) at a growth temperature of 20 °C. The above procedure is different from that of our initial static LLIP method without the manual mixing process [3]. C_{60}NWs were synthesized for various volume ratios of the C_{60}-saturated toluene solution to IPA between 1:7 and 7:1. Toluene to IPA ratio in the volumetric proportion (x:y) is designated as xTy I.

The length and diameter of C_{60}NWs were measured by optical microscopy (Nikon ECLIPSE ME600) and scanning electron microscopy (SEM, JEOL JSM-6700F) for exactly 100 C_{60}NWs in each sample.

2.2. Synthesis of C_{60}NWs using isopropyl alcohol added with water

The addition of water to the C_{60}–toluene–IPA solution was performed by use of IPA added with distilled water (Wako Pure Chemical Industries, Ltd., Japan). The volume ratio of the C_{60}-saturated toluene solution to the IPA containing water was set to be 1:1. The content of water in IPA was set to be less than 2.5 mass % H_2O.

The formation of liquid–liquid interface and the mixing of solutions were similarly performed as shown above. Instead of H_2O, heavy water (D_2O, ISOTEC, 99.96 at%) was also used to study the effect of water on the growth of C_{60}NWs for comparison. The growth experiments were performed between 5 and 20 °C. In this paper, "water" normally means H_2O as long as no special notice is indicated.

3. Results and discussion

3.1. Effect of solvent ratio on growth of C_{60}NWs

Fig. 1 shows the glass bottles observed immediately after the manual mixing and those 24 h after the manual mixing. The opaque glass bottles 1T3I, 1T1I and 3T1I of Fig. 1(a) became transparent 24 h after the manual mixing and the highest yield of C_{60} precipitates is observed in the bottle of 1T1I. The purple color observed in the glass bottles of 1T1I–7T1I shows the excess C_{60} molecules dissolved in the solutions, which shows that an appropriate amount of IPA is necessary to attain complete precipitation of C_{60} crystals.

On the other hand, as shown in Fig. 2, granular precipitates other than C_{60}NWs were observed in the samples prepared by use of the solutions of 1T7I, 1T5I and 3T1I. Examples of the granular crystals are indicated by the white arrows. Although those granular crystals became less with increasing the toluene content as shown in the SEM images of 1T5I, 1T3I and 1T1I, only granular precipitates like those in Fig. 2(e) were formed in the solutions of 3T1I, 5T1I and 7T1I. This fact shows that an optimum solvent ratio exists for the growth of C_{60}NWs. Especially, the C_{60}NWs of 1T1I show the best developed linear morphology and no granular precipitates are found.

The formation of granular particles means isotropic crystal growth of C_{60}. The modes of isotropic crystal growth and anisotropic crystal growth of C_{60} are strongly related with the solvent ratio as discussed later.

Fig. 3 shows the relationship between length and diameter of C_{60}NWs for the four solvent ratios of 1T7I, 1T5I, 1T3I and 1T1I.

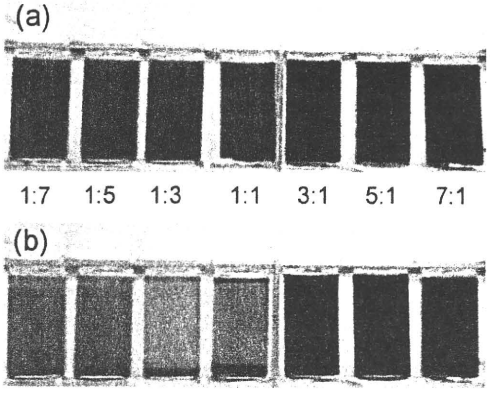

Fig. 1. (a) Glass bottles observed immediately after the manual mixing and (b) those observed 24 h after the manual mixing at the growth temperature of 20 °C.

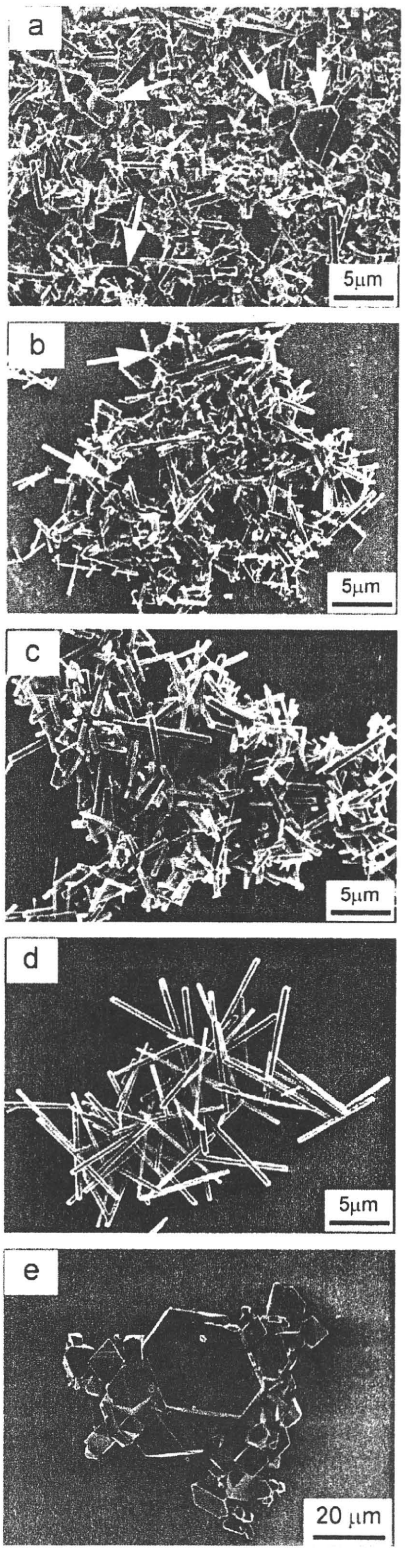

Fig. 2. SEM micrographs of the C_{60}NWs grown for 24 h by use of the solutions with different volume ratios of C_{60}-saturated toluene and IPA at 20 °C. Toluene: IPA (v/v)= (a) 1:7, (b)1:5, (c) 1:3, (d) 1:1 and (e) 3:1.

The best grown C_{60}NWs are shown in Fig. 3(d) of 1T1I, corresponding to the image of Fig. 2(d). On the other hand, diameter of the C_{60}NWs shows large scatter about length of the

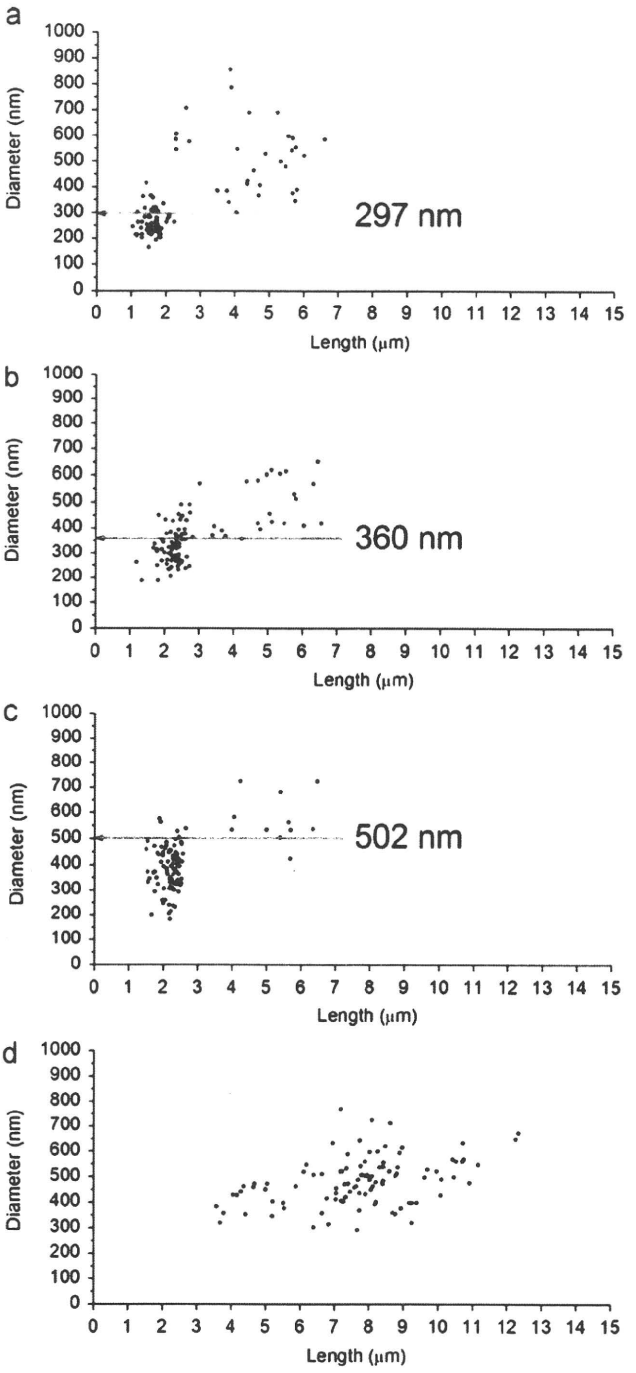

Fig. 3. Relationship between length and diameter of C_{60}NWs synthesized at different solvent volume ratios of toluene and IPA for the growth time of 24 h at 20 °C. Toluene: IPA (v/v)= (a) 1:7, (b) 1:5, (c) 1:3 and (d) 1:1.

C_{60}NWs. Moreover, it is noted that there is a critical diameter (D_c) above which the length of the C_{60}NWs increases, i.e., the whisker length becomes significantly larger above the critical diameters hypothetically set at 297 nm (b), 360 nm (c) and 502 nm (d). This fact shows that the crystal nuclei of C_{60} grow isotropically for the diameters less than D_c and grow anisotropically for diameters greater than D_c. In the solution-grown crystals, it is generally accepted that the crystals can grow above a critical radius R_c that is determined by supersaturation of the solution at a given temperature [37].